iScience

CellPress
OPEN ACCESS

Article

Spatial clustering of orientation preference in primary visual cortex of the large rodent agouti

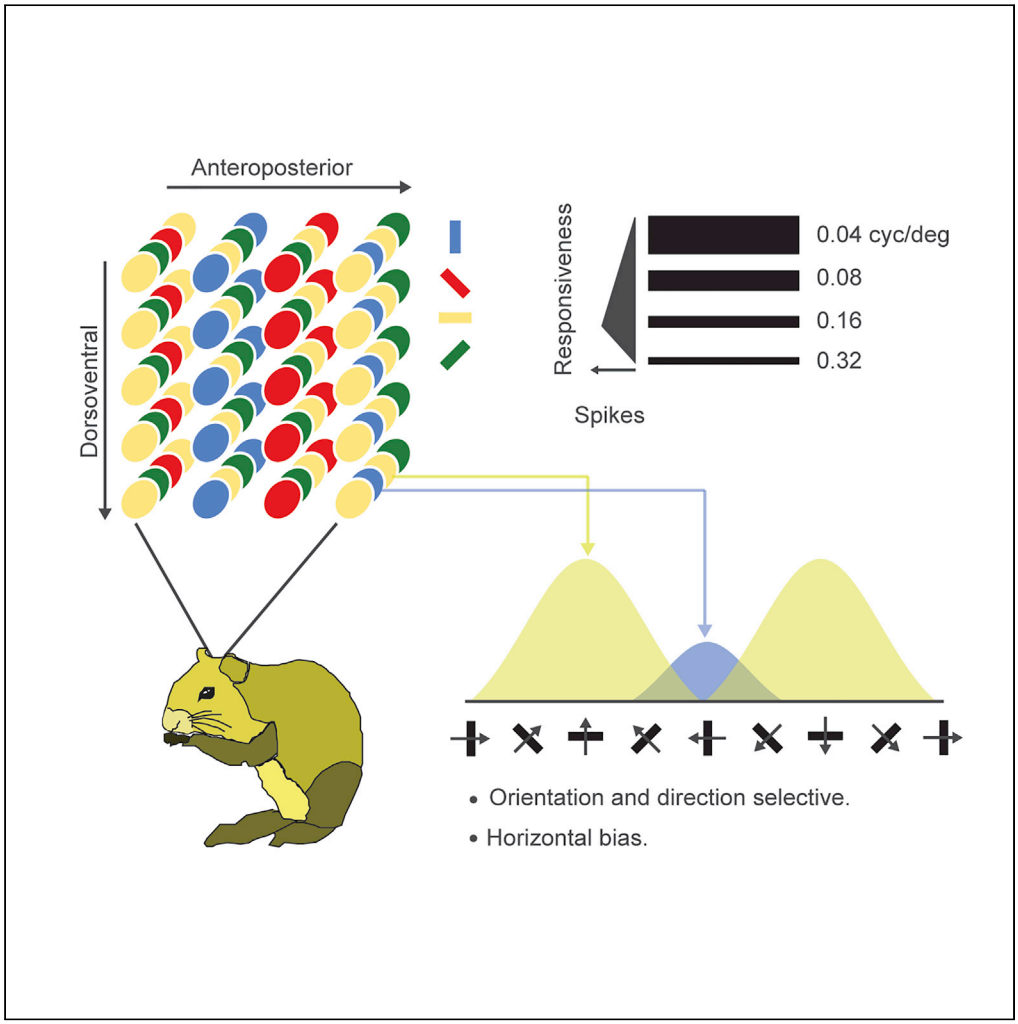

Dardo N. Ferreiro, Sergio A. Conde-Ocazionez, João H.N. Patriota, Luã C. Souza, Moacir F. Oliveira, Fred Wolf, Kerstin E. Schmidt

kschmidt@neuro.ufrn.br

HIGHLIGHTS

Agouti V1 neurons are among the highest orientation- and direction-selective neurons in rodents

They respond best to low spatial frequencies and with a bias for horizontal orientations

There is no evidence of systematic periodic maps of orientation columns for agouti

Neurons along the vertical cortical axis tend to have similar orientation preferences

Ferreiro et al., iScience 24, 101882
January 22, 2021
https://doi.org/10.1016/j.isci.2020.101882

iScience

CellPress
OPEN ACCESS

Article

Spatial clustering of orientation preference in primary visual cortex of the large rodent agouti

Dardo N. Ferreiro,[1] Sergio A. Conde-Ocazionez,[1,2] João H.N. Patriota,[1] Luã C. Souza,[1] Moacir F. Oliveira,[3] Fred Wolf,[4,5,6,7] and Kerstin E. Schmidt[1,8,*]

SUMMARY

All rodents investigated so far possess orientation-selective neurons in the primary visual cortex (V1) but – in contrast to carnivores and primates – no evidence of periodic maps with pinwheel-like structures. Theoretical studies debating whether phylogeny or universal principles determine development of pinwheels point to V1 size as a critical constraint. Thus, we set out to study maps of agouti, a big diurnal rodent with a V1 size comparable to cats'. In electrophysiology, we detected interspersed orientation and direction-selective neurons with a bias for horizontal contours, corroborated by homogeneous activation in optical imaging. Compatible with spatial clustering at short distance, nearby neurons tended to exhibit similar orientation preference. Our results argue against V1 size as a key parameter in determining the presence of periodic orientation maps. They are consistent with a phylogenetic influence on the map layout and development, potentially reflecting distinct retinal traits or interspecies differences in cortical circuitry.

INTRODUCTION

Many early sensory cortical areas are orderly arranged in functional structures, where neurons sharing similar response properties lie close to each other. A well-described example is the organization of orientation-selective neurons into domains or columns of iso-preference in the primary visual cortex. Like receptive field position, orientation preference is preserved along the axis perpendicular to the cortical surface but changes systematically around singularities in the axis parallel to it, forming pinwheel-like structures. Therefore, the same preferred orientation repeats in area-specific intervals forming regular orientation preference maps (OPMs) that have been found in V1 and V2 of all carnivores (e.g. Bonhoeffer and Grinvald, 1991; Hubel and Wiesel, 1962; 1963; Chapman et al., 1996), primates (e.g. Essen and Zeki, 1978; Hubel and Wiesel, 1968; Ts'o et al., 1990; Blasdel and Salama, 1986), and their close relatives (see Kaschube et al., 2010) studied so far. Although all investigated rodent species presented orientation-selective neurons, no such maps have been observed in this order (rats: Ohki et al., 2005, gray squirrel: Van Hooser et al., 2005, mice: Bonin et al., 2011). This lack of classical columns gave rise to the terms "interspersed" or "salt-and-pepper" organization implying a random spatial arrangement of orientation-selective neurons in these animals. Noteworthy, reports in lab mice (Ringach et al., 2016; Kondo et al., 2016) and grasshopper mouse (Scholl et al., 2016) indicate that the arrangement is not entirely random. Instead, these authors describe functional modules of roughly 30 μm diameter which run perpendicular to the cortical surface and contain neurons tuned to similar orientations, which they thus termed "mini-columns". Along this line, several studies, mostly theoretical, have proposed that the formation of OPMs might not be solely dependent on phylogeny but might be due to self-organization (Kaschube et al., 2010), constrained by factors such as brain size (Keil et al., 2012; Meng et al., 2012), number, and density of neurons (Weigand et al., 2017). The main argument behind these ideas is that, within bigger and more neuron dense cortical areas, an interspersed organization imposes higher wiring costs than periodic orientation columns. Since neurons that respond to similar preferences tend to interconnect (i.e. Löwel and Singer, 1992; see also Hebb, 1949), shorter axons with closer pathways and faster signal transmission between those neurons might be achieved through a more periodic spatial arrangement of orientation selectivity when assuming a dynamical map formation (Wolf and Geisel, 1998; Koulakov and Chklovskii, 2001). According to this argument, for bigger brains, it would be more efficient to cluster their neurons by functional similarity in modules as observed in OPMs (for review see Chklovskii and Koulakov, 2004).

[1]Neurobiology of Vision Lab, Brain Institute, Federal University of Rio Grande do Norte, Natal, Brazil

[2]Universidad de Santander, Facultad de Ciencias de la Salud. Laboratorio de Neurociencias, Bucaramanga, Colombia

[3]Department of Veterinary Medicine, Universidade Federal Rural do Semiárido, Mossoró, Brazil

[4]Max Planck Institute for Dynamics and Self-Organization, Göttingen, Germany

[5]Bernstein Center for Computational Neuroscience, University of Göttingen, Göttingen, Germany

[6]Max Planck Institute of Experimental Medicine, Göttingen, Germany

[7]Campus Institute for Dynamics of Biological Networks, University of Göttingen, Göttingen, Germany

[8]Lead Contact

*Correspondence: kschmidt@neuro.ufrn.br

https://doi.org/10.1016/j.isci.2020.101882

Not surprisingly, given their availability, all rodents studied so far have been of smaller brain size and of nocturnal (mice, rats) or crepuscular habits (gray squirrels). The theoretical considerations above predict that rodents with a larger V1 size such as agouti and capybara might present OPMs (Weigand et al., 2017). Thus, we set out to study the functional responses and anatomical layout of orientation-selective neurons in the red-rumped agouti *Dasyprocta leporina*. Agoutis are diurnal rodents native to South and Central America with body and brain size comparable to that of cats. Their V1 surface extends for over a centimeter lateral from the lateral sulcus and even longer in the antero-posterior axis and spans around 320–340 mm^2 (Dias et al., 2014; their Figure 2; personal communication M. Garcia). Although the agouti's retinotopic layout has been studied before (Picanço-Diniz et al., 1991), no orientation selective visual responses of this species were ever recorded. In the present study, we obtained maps of retinotopy and orientation-selective responses from intrinsic signal imaging. Subsequently, we quantified receptive field size in detail and neuronal response tuning to several stimulation parameters such as contour orientation, direction of movement, and spatial and temporal frequency (TF) from *in vivo* parallel electrophysiological recordings in the anesthetized agoutis' visual cortex. We used vertical and horizontal grids of multi-electrodes to determine the topographic layout of orientation selectivity. The same experiments were performed in anesthetized cats (Brodmann areas 17 and 18) in order to directly compare agouti neuron selectivity and layout with the well-established cat model.

RESULTS

Guided by Dias et al. (2014), we identified the anatomical location of V1 in agoutis and performed extracellular electrophysiological recordings from single units and optical imaging of intrinsic signals. V1 identity was histologically confirmed postmortem. In order to compare our results in the novel rodent species to a well-established non-rodent model with similar V1 size, we also performed the same experiments in cats.

Receptive field size

Agoutis possess a visual streak (Figure 1A, Picanço-Diniz et al., 1991) and laterally positioned eyes. Therefore, we mapped and evaluated the area (see Transparent Methods) of the aggregate classical receptive fields (aCRF) based on multi-unit activity as a function of eccentricity by stimulating monocularly in the range between 5 and 118°. In cats, we stimulated binocularly after aligning the eyes using an optic prism. Although we did not record central binocular responses in the agouti, we still obtained a considerable overlap in the eccentricities of the aCRF recorded in both species. Agoutis can have small receptive fields at a wide range of eccentricities (Figure 1B).

All the units recorded had aCRFs close to the horizontal meridian of the visual field ($\pm$15° in elevation) (Figures 1C–1E). We quantified the area of multi-units with well-defined aCRFs (n = 401 in agouti, n = 125 in cat A18, n = 82 in cat A17). Our measurements for agouti aCRF size are in the 1–22 deg^2 range. Cat A18 aCRF sizes are in the 1–32 deg^2 range, and A17 aCRF sizes are in the 0.5–22 deg^2 range. Agouti aCRF sizes are much more similar to cat A17 than cat A18 sizes (mean and SD values: cat A17 = 7.2 $\pm$ 4.3; cat A18 = 11.5 $\pm$ 6.5; agouti V1 = 6.2 $\pm$ 3.7; Figure 1F).

Cat area 18 exhibits bigger CRFs (2–32 deg^2 range reported in (Hubel and Wiesel, 1965)) and selectivity to lower spatial frequencies (SFs) than area 17 (Movshon et al., 1978). Characteristically, for cat area 18, it can be observed that the cat's aCRF size increases rapidly with elevation and eccentricity (Figures 1C and 1E) while the agoutis' aCRFs remain small at large eccentricities of up to 120° (Figure 1F).

Orientation and spatial frequency selectivity

Previous studies (Picanço-Diniz et al., 1991; Dias et al., 2014) recorded retinotopic visual responses in agouti V1, but orientation selectivity in this species has not been reported yet. Thus, we used drifting sine wave gratings to characterize functional visual responses. The gratings consisted of twelve directions of movement, three TFs (2, 4, and 8 Hz), and seven SFs (0.04, 0.08, 0.16, 0.32, 0.64, 1.28, and 2.56 cpd). Single units that passed a sign test with a 95% confidence interval ($p < 0.05$) between their pre-stimulus and evoked firing rates were considered visually driven and included in the analysis. Agouti neurons fired more vigorously at 0.08 and 0.16 cpd (see Figure 3A) and ceased to respond reliably to higher SFs than 0.64 cpd at all TFs tested. They further responded much less selectively to 8Hz < 4 Hz < 2 Hz stimulation. For stimulation with 8 Hz, we encountered almost no visually driven cells and with 4 Hz much less than with 2 Hz, which met our selectivity criterion (see below). In addition, the few selective responses obtained at 4 or 8 Hz did not behave qualitatively different than at 2 Hz for different SFs. Thus, in the following comparative and spatial analysis, we focused on data obtained at 2 Hz and at SFs <0.64 cpd.

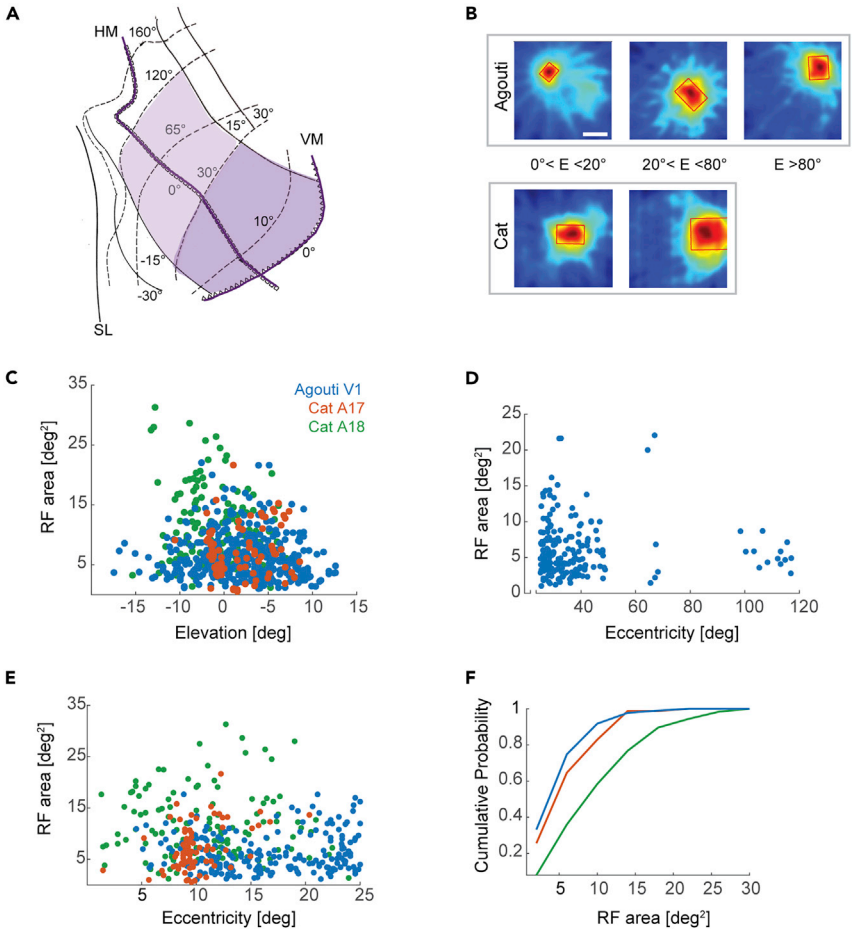

Figure 1. Receptive field size in agoutis and cats

(A) Sketch of the electrophysiologically sampled area in agouti V1.

(B) aCRF mapping examples from agouti V1 at three different eccentricities (E) along the visual streak (elevation less than 5°) and two fields from cat area 18. Scale bars represent 2°.

(C) Receptive field size as a function of elevation. Data from 5 cats and 11 agoutis: 125 multi-units for cat A18, 82 for cat A17, and 401 for agouti V1.

(D) Receptive field size as a function of eccentricity. More lateral part of the visual streak in agouti (light violet shade in A, 30–120 deg). Agouti aCRFs do not increase at large eccentricities (≥90 deg).

(E) Receptive field size as a function of eccentricity. Zoom into the central visual field <25 deg (dark violet shade in A).

(F) Cumulative distributions of aCRF size for agouti V1, cat area 17, and 18. Note that agouti V1 neurons tend to have aCRFs of similar size as cat area 17.

SL, lateral sulcus; HM, horizontal meridian; VM, vertical meridian. Cortical coordinates: M, medial; L, lateral; A anterior; P, posterior; adapted from Picanço-Diniz et al. (1991).

Some examples of response profiles of single units to several orientations and directions are depicted in Figures 2A and 2B (for peri-stimulus time histograms (PSTHs) see Figure S3). We computed, based on each profile, an orientation selectivity index and a direction selectivity index (OSI and DSI, respectively,(-Wunderle et al., 2013) (Conde-Ocazionez et al., 2018), and see Methods), where an index of 1 indicates a neuron that responds to only one stimulus orientation or direction, and an index of 0 indicates equal responsiveness across all orientations or directions.

For the quantitative comparison of cell populations between both species, the best OSI or DSI obtained per single unit for a given SF was considered (Figures 2C and 2D). This was done in order to count each single unit's OSI and DSI once and at its optimal stimulation. In addition, only single units fulfilling the criteria of (i) a positive sign test, (ii) a significant OSI, i.e., above the spike-dependent OSI threshold

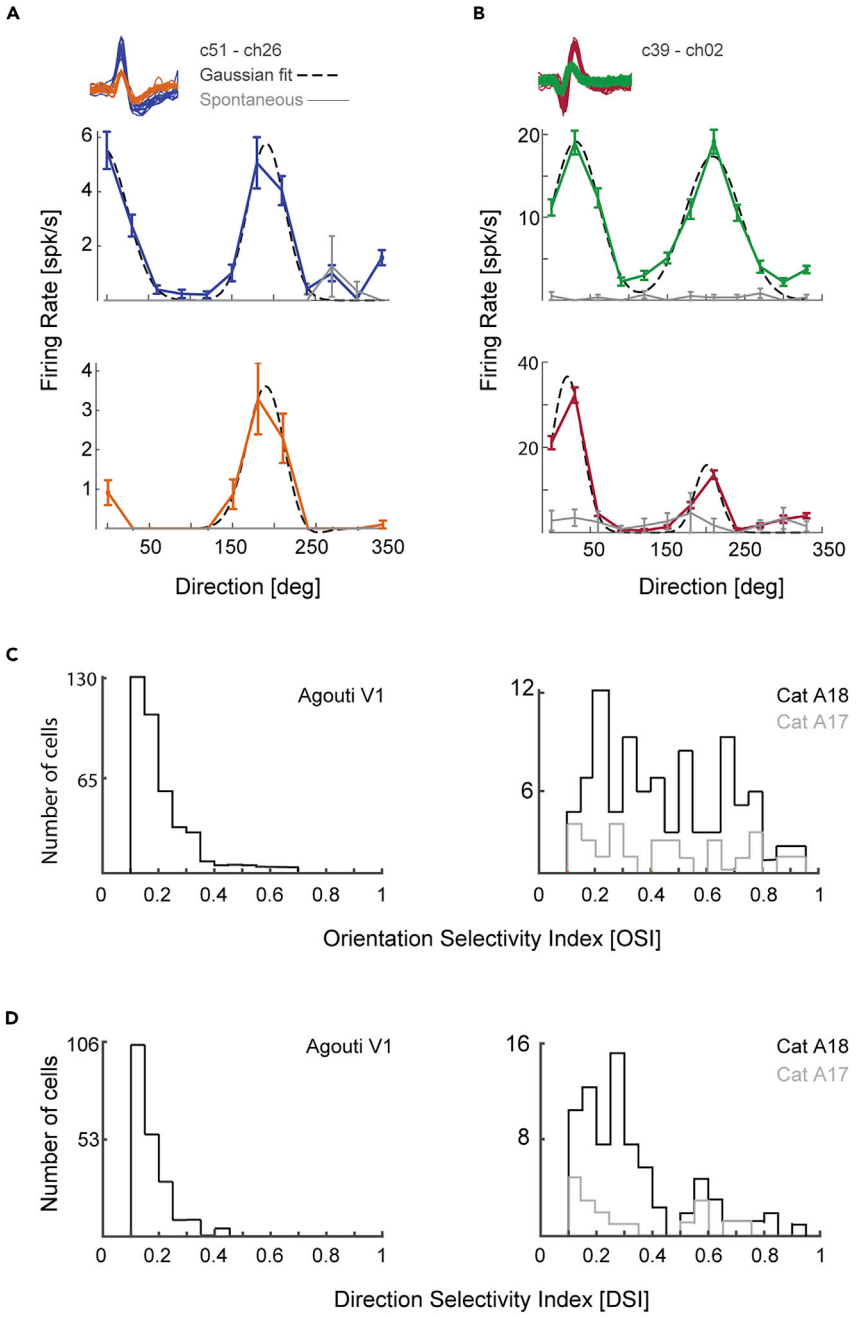

Figure 2. Orientation selectivity in primary visual cortex of agouti and cat

(A and B) Examples of isolated units for agouti (A) and for cat area 18 (B) stimulated at 0.08 cpd. Dashed lines indicate double Gaussian fits to the mean firing rates. Light gray lines indicate pre-stimulus firing rate. Error bars, standard deviation. Note that here agouti and cat units prefer the horizontal direction of movement and have thus vertical orientation preference.

(C) Distributions of orientation selectivity indices (OSIs) in both species. Agouti selectivity indices (n = 349) are significantly lower than indices for cat area 18 (n = 97, Mann-Whitney U, $p < 0.0001$) and cat area 17 (n = 22, Mann-Whitney U, $p < 0.0001$).

(D) Distributions of direction selectivity indices (DSIs) in both species. For (C and D), cat distributions of OSI and DSI are divided into Brodmann areas 17 (gray) and 18 (black). Only indices of neurons that passed both the spike-dependent threshold and a static threshold of 0.1 are depicted. Error bars are SEM (standard error of the mean).

(Figure S2), (iii) with an OSI greater than a static threshold of minimum 0.1 were considered (see Wunderle et al., 2013; Peiker et al., 2013 for similar selection criteria).

Overall, agouti selectivity indices in this sample are significantly lower than those of cats with a median OSI for agouti V1 at 0.2 (n = 349), for cat A18 at 0.43 (n = 97), and for cat A17 at 0.43 (n = 22) (Mann-Whitney U, $p < 0.0001$ for both comparisons between agouti V1 and cat A18 or cat A17).

Though the difference between the species is smaller for the DSI than the OSI distributions, agouti neurons are notably less direction selective than those of cat area 18 (Figure 2D). For DSIs selected according to the same criteria (crossing the spike-dependent DSI threshold and a static DSI threshold of minimum 0.1), the median DSI for agouti V1 in the sample is 0.17 (n = 261), for cat A18 is 0.25 (n = 91), and for cat area 17 is 0.21 (n = 18) (Mann-Whitney U, $p = 0.04$ for the comparison between agouti V1 and cat A18).

Although the spike-dependent threshold corrects for high indices, which are rate related, we also checked whether agouti indices might be lower because of lower absolute firing rates and thus lower signal-to-noise ratio caused by anesthesia. To this end, we compared median OSI indices between rate-matched samples of the two species (OSI >0.1, 10 sps < evoked rate <20 sps). The result supports the conclusion that the difference in selectivity between the two species is not related to firing rate (median OSI agouti V1, 0.16, n = 91, versus median OSI cat area 18, 0.36, n = 21; Mann-Whitney U $p < 0.0001$).

In addition to the OSI, we further calculated the classical orthogonal modulation depth index (OMDI) of orientation selectivity (see Methods, e.g. Niell and Stryker, 2008; Mazurek et al., 2014). Accordingly, we calculate 0.3 for agouti V1 neurons, 0.63 for cat A18, and 0.49 for cat A17 (see Bachatene et al., 2016, for similar values). Having excluded extreme indices of 1 because of 0 firing in the opposite directions, median OMDIs are still higher than the spike-rate-dependent OSIs but highly significantly correlated with them (Wilcoxon signed rank, $p < 0.0001$). So, both species differences and also the dependence of orientation selectivity on SF (data not shown) remained similar. In addition, the angle of the grating direction, which evoked the optimal response, differed only $11.4 \pm 9.4°$ from the preferred angle obtained by vector summation.

Although the population of agouti neurons responded over a broad range of SFs, they fired more vigorously at lower SFs (Figure 3A) with most of the neurons exhibiting highest firing rates at 0.08 cpd (Figures 3B and 3C). Orientation-selective firing could be observed up to 0.64 cpd (Figure 3D). Since SF and orientation tuning have been observed not to be independent response characteristics in cats (e.g. Jones et al., 1987), we investigated whether the degree of orientation selectivity of agouti neuron responses varied as a function of SF.

Although OSI values of agouti single units crossing the threshold are much lower and less modulated with SF than those of cat neurons (Figures 3F and 3G), the mean OSI of the those responses presents a SF tuning profile with a peak for 0.32 cpd (Figure 3G). The cat SF profiles are congruent with the cat literature (i.e. Ribot et al., 2013). For example, as expected, 0.64 cpd stimulation still produced highly selective responses for cat area 17 (Figure E, F) but not for cat area 18 (Figure 3F).

In addition to the OSI and DSI values, we computed the half-width at half-height (HWHH) of the orientation and direction tuning curves of agouti neurons.

This parameter quantifies the sharpness of the orientation or direction tuning curves, as third selectivity indicator, by fitting the normalized firing rate responses to Gaussian curves (Figure 4A, also see Methods). In this analysis, we only considered neurons with an orientation (for orientation HWHH) or direction (for direction HWHH) selectivity index higher than 0.2.

In comparison to cats, we found for orientation (Figure 4B) and direction tuning curves (Figure 4C), larger HWHH values for agouti units than for cat units, reflecting broader tuning curves (as depicted in the examples in Figure 4A).

The discrepancy between HWHH values of the two species is particularly high for direction selectivity. As expected for area 18 (Orban et al., 1981), these neurons are well tuned for direction of motion, and thus, the direction tuning curves are very narrow.

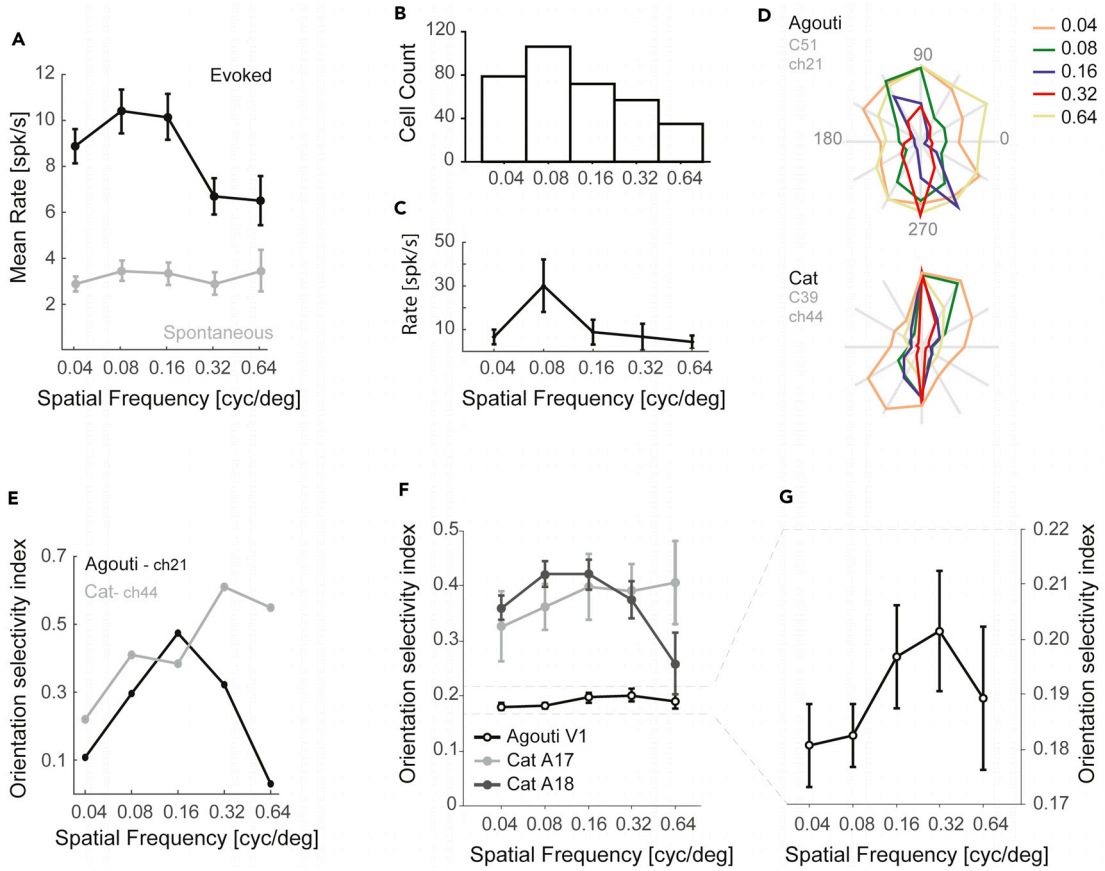

Figure 3. Agouti V1 neurons are selective for spatial frequency

(A) Population mean firing rate of all orientation-selective agouti single units evoked at different spatial frequencies (black line) and during the pre-stimulus period (gray line).

(B) Counts of neurons that evoked maximum mean firing rate at that SF.

(C) Spatial frequency tuning curve example. Mean maximum firing rate obtained with an optimal grating at each SF. Error bars, standard deviation.

(D) Polar plot of the example agouti single unit (upper) and of a cat area 17 single unit (lower) at five different SFs.

(E) Orientation selectivity index of the two neurons of D at different SFs. Note that the agouti neuron fires most at 0.08 and exhibits highest orientation selectivity at 0.16 cpd. For comparison, the cat area 17 neuron remains selective at high SFs.

(F) Spatial frequency selectivity of the mean orientation selectivity indices for agouti, cat A17, and cat A18 in the same scale.

(G) Same as (F) zooming in on the agouti curve. Note that agoutis show small orientation selectivity indices, with optimal OSI tuning at 0.32 cpd in the visual area investigated. Only indices of neurons that passed both the OSI spike-dependent threshold and a static threshold of 0.1 were included (n = 349). Error bars are SEM (standard error of the mean), except for (C)

We further observed that agouti orientation HWHH is in accordance with what was reported for the gray squirrel, the only other large visual rodent studied so far (<70 deg, Van Hooser et al., 2005). Noteworthy, in the cited study, a more rigid criterion (OSI >0.5) was applied to sample the orientation-selective units from which the HWHH was calculated. With such a high threshold, Van Hooser et al. (2005), report a median HWHH of 28 deg. Therefore, we repeated the HWHH in our data for cells with an OSI >0.5 and obtained an agouti median HWHH for orientation tuning lower than 23 deg for all of the five SFs studied (similar results for cats, data not shown). Although not conclusive, agouti neurons seem to have a sharper orientation tuning than the gray squirrel neurons.

Spatial layout of orientation selective neurons

In order to analyze the spatial layout of neurons with similar orientation preference, we analyzed their differences in orientation preference as a function of cortical distance. Preferred angle differences may range from 0 deg to 90 deg.

We compared this measure for the same type of recordings in agoutis and cats. For a salt-and-pepper-like layout, the angle difference between pairs of neurons should be independent of the cortical distance. In

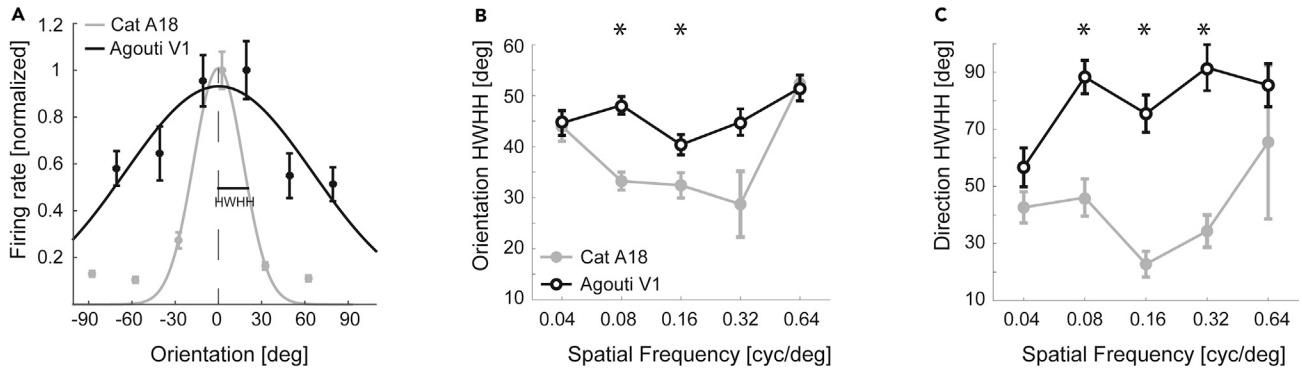

Figure 4. Sharpness of orientation and direction tuning curves in agoutis and cats

(A–C) (A) Examples of Gaussian fits of orientation tuning curves elicited at 0.32 cpd for one agouti and one cat single unit. Mean population half-width at half-height (HWHH) of orientation (B) and direction (C) selectivity tuning curves. Firing rates for each stimulation orientation/direction were normalized for every neuron with a selectivity index >0.2. A single peak Gaussian function was fitted to each of the normalized firing rates for orientation/direction, for each spatial frequency. Note that tuning curves of cat area 18 neurons have much lower HWHH values than agouti, especially for direction selectivity. Data from 2 cats and 9 agoutis. Error bars: SEM. Stars indicate significant differences between agoutis and cats (Wilcoxon rank-sum test; $p < 0.001$; n = agouti units, cat units)

contrast, for periodically repeating orientation columns that compose orientation preference maps as in cats, the angle difference between pairs of neurons should increase smoothly with distance in all directions parallel to the cortical surface until targeting the proximal domain of orthogonal orientation preference. Similarly, this difference should be minimal when comparing adjacent cells, as within a cortical column or at the same electrode.

It should be noted that all cortical distances shown in Figure 5 are distances between the electrodes at which the two neurons being compared were recorded. Therefore, the distances declared here are not exact neuronal distances but a close estimate. Whenever a comparison is declared to be of 0 μm distance, it means that the two neurons were recorded from the same electrode. In Figures 2A and 2B, we illustrate that clearly different waveforms from the same multi-unit with similar orientation tuning could be isolated in both species.

Figure 5A displays the angle differences as a function of horizontal cortical distance for pairwise cell comparisons, considering the orientation preference obtained with the SF that elicited the highest OSI. For comparisons of distances equal or greater than 250 μm, agouti orientation preference differences do not deviate from the estimate for a random spatial layout (dotted gray line, shuffled data). In contrast, the cat's angle difference profile shows the expected smooth increase of angle differences across cortical distance with a characteristic valley around 900 μm roughly corresponding to the distance between iso-orientation columns. This indicates a structure in cats' OPMs which agoutis lack. However, the result that agouti angle differences deviate significantly from the shuffled data at 0 μm is compatible with the interpretation that neurons recorded from the same electrode do have similar orientation preference, implying a local structure (see also Figure 6A).

In Figures 3 and 4, we had observed that orientation selectivity indices of agoutis are much lower and tuning curves are more flat than those of cats. This opens the question whether the calculated preferred orientation is actually able to accurately reflect the overall functional layout in those animals.

Therefore, we aimed for a measure, which takes not only the difference between "best angles" into consideration but also the shape of each cell's tuning curve. To accomplish this aim, we calculated the orientation tuning similarity, which is the Pearson correlation between the orientation tuning curves (i.e. the firing rates to each stimulus orientation; see Methods) of the two neurons to be compared (Figure 5B, see also plots separated by SF in Figure S4)

For both cat and agouti, the Pearson correlation reaches its positive peak at the smallest comparable distance. For agoutis, the maximum correlation obtained is only 0.5, drops to the shuffled data mean already at the next available distance point, and stays constant across the remaining distances. For cats, the correlation starts at much higher values (0.7), reaches negative correlation values, and also exhibits the

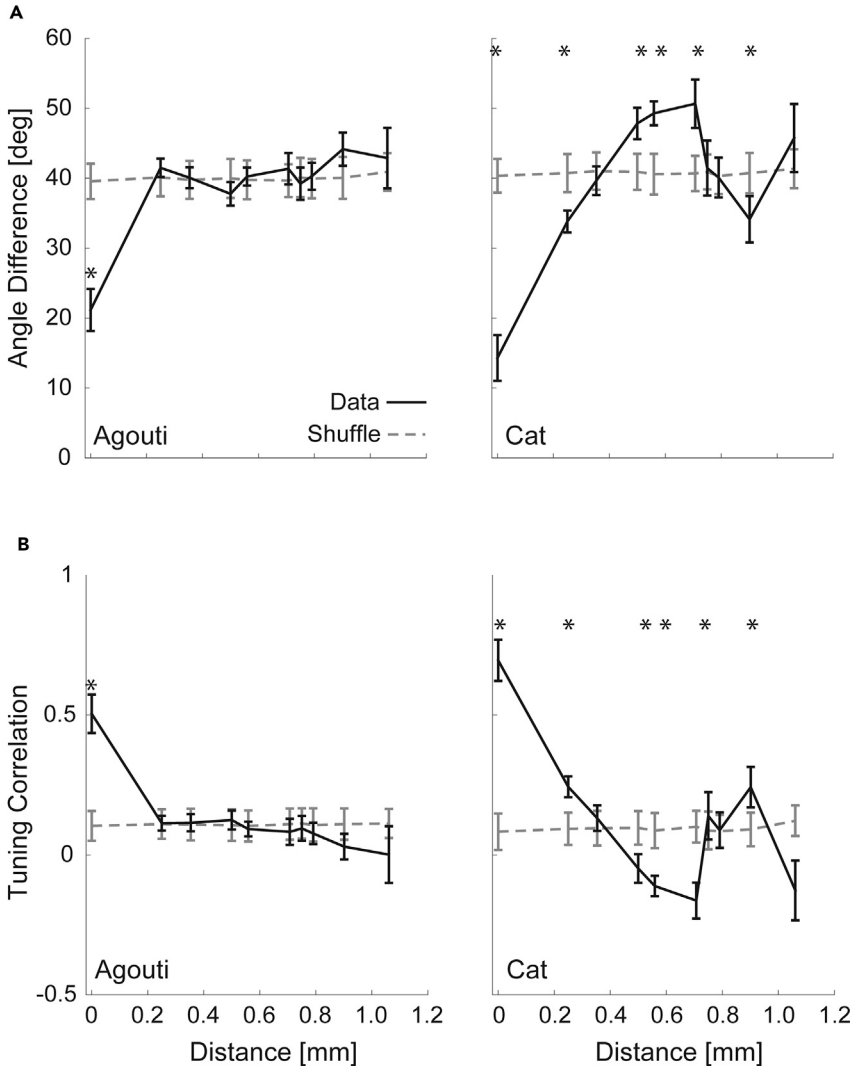

Figure 5. Spatial layout: tuning difference between cell pairs as a function of distance

Mean pairwise angle difference (A) and pairwise Pearson correlation of firing rates to stimulation angle (B) as a function of horizontal cortical distance for cat A18 and agouti V1. For each cell, only the orientation preference at the spatial frequency, which elicited the highest OSI, was considered. Gray dotted lines represent the calculation for the shuffled data. Asterisks depict significant differences between the correlations obtained for recorded and shuffled data. Significance criterion: Mann-Whitney $p < 0.001$ (Bonferroni correction for 10 multiple comparisons) for the pairwise comparison of the data points and the shuffled data. Data from 2 cats and 5 agoutis. For raw p values, see Tables S1 and S2, for number of data points, see Table S3. Note that agouti neuron similarity is only different than chance for neurons that lie close to each other. Error bars: SEM.

characteristic reversion around 900 μm, already discussed above for the "angle difference" measure. Here, similar to both measures of angle difference and tuning similarity, we observe a maximum negative difference in neuronal similarity at around 700 μm. This is to be expected as the distance between cross-orientation columns in cat area 17 is approximately 500 μm and a little bit larger in area 18 (e.g. Löwel et al., 1987).

From these plots, we draw the conclusion that agouti neurons situated very close to each other (i.e. were recorded within the same electrode) have a higher feature similarity than expected by chance, but this does not hold for neurons recorded at different recording sites. Noteworthy, the agouti's tuning correlation also never reaches negative values, suggesting that clearly segregated domains of orthogonal orientation preference at such regular intervals as known for cat orientation preference maps, for example, are rather unlikely.

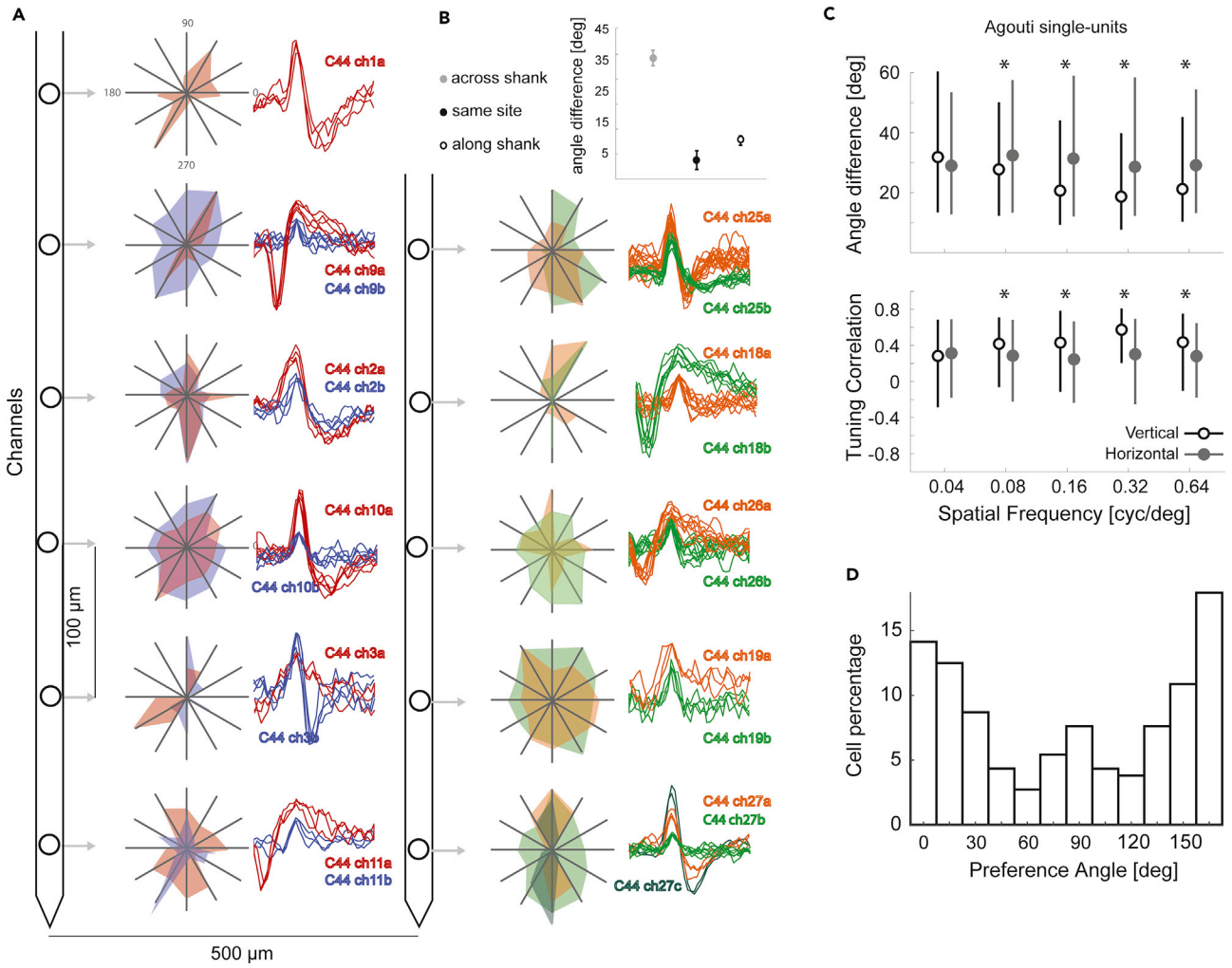

Figure 6. Orientation preference distribution across vertical and horizontal dimensions

(A) Polar plots of example single units recorded from a vertical double shank probe at 0.08 cpd. Waveforms from separated units are color coded. Note that orientation preference in agoutis is relatively stable along the vertical axis. Representatively, units on both shanks prefer orientations varying around the horizontal axis.

(B) Angle differences are higher across (gray filled circle, n = 121) than along shanks (empty circle, n = 145; Mann-Whitney-U, $p < 0.005$) and between units separated from the same site (black filled circle, n = 24; Mann-Whitney-U, $p < 0.0001$).

Pairwise differences (C) Pairwise comparisons of orientation preference across all electrodes of each device. Median and interquartile ranges are depicted by circles and lines, respectively. Empty and filled circles depict pairwise comparisons between single units from Neuronexus probes or electrode arrays, respectively. Probe electrode sample from a vertical cylinder (A, orthogonal to cortical surface). Array sample from horizontal planes (parallel to cortical surface). Angle difference (top) and tuning similarity (bottom). Both measures indicate a greater similarity between neurons arranged vertically. * depicts $p < 0.0001$ (Mann-Whitney U test, for raw p values see Tables S4 and S5). Probe electrode data from 3 agoutis. Array electrode data from 5 agoutis.

(D) Percentage of agouti single units with different orientation preferences above selectivity threshold categorized in 12 groups of $\pm$7.5 deg at 0.16 cpd and 2 Hz (n = 85 neurons). Strikingly, in the overall sample, the horizontal orientation preference predominates.

Clustering of iso-orientation cells in agouti V1 along the vertical axis and orientation bias

Inspired by the above results and the "mini-column" findings in the rodent visual cortex in the recent years (Ringach et al., 2016; Kondo et al., 2016; Maruoka et al., 2017), we investigated if the orientation preference similarity of nearby single units holds along the axis perpendicular to the cortical surface. To this end, we recorded with vertical probe electrodes with 16 recording sites of 100-µm inter-site distance inserted perpendicularly to the cortical surface (Figure 6A). We observed that the orientation preference of single units along the shank tended to be more similar than between two shanks spaced 500 µm apart (Mann-Whitney-U test, along versus across shanks, n = 222, $p < 0.0001$ Figure 6B).

Thus, we also statistically compared angle differences and tuning similarity of all single unit pairs either along the probe shank dimensions (Figure 6C, black empty circles, perpendicular to the cortical surface) or across the array dimension (gray full circles, parallel to the cortical surface). For both types of electrodes and each SF analyzed, the angle difference (Figure 6C, top) and tuning similarity (Figure 6B, bottom) were calculated between all recording sites of a probe or an array where an orientation selective unit response was recorded.

For the majority of tested SFs, angle differences were significantly smaller along the vertical than the horizontal dimension indicating greater similarity of orientation preferences of different recording sites in depth. In accordance, the similarity index was also significantly greater for neurons along the vertical dimension. It seems that neurons of similar orientation preference are grouped together on a short-range scale in a columnar-like manner but that orientation preference is not organized periodically across the horizontal plane.

In further support of this observation, the same result is obtained when analyzing the spatial layout among multi units (Figure S5).

Strikingly, in the example of Figure 6A, close to horizontal orientation preferences (slightly left oblique for shank 1 and right oblique for shank 2), seem to dominate for units both along and across the two shanks. Although units responding to vertical contours also occurred (see Figure 2A), the example recording matches an overall bias in the sample of agouti units preferring stimulation with horizontal contours (Figure 6D). When separating units according to their orientation preference at 0.16 cpd in 12 categories of equal size ($\pm$7.5 deg), the majority of units express horizontal preference.

Variation of preferred orientation across spatial frequency

In the previous section, we established the similarity of orientation preferences of neurons (inter-neuronal comparison) by comparing their preferred angle at the SF, which elicited the highest OSI. Next, we investigated the stability of the preferred angle of selective neurons across SFs of stimulation (intra-neuronal comparison). It turned out that agouti – in contrast to cat – orientation preference varies considerably across SFs (Figure 7A). Thus, we analyzed the stability of angle preference for every neuron that showed an orientation-selective response above the threshold to at least two SFs. We used two metrics of preferred orientation dispersion, namely, the angle range (Figure 7B, top), which is the largest difference in the preferred angles of all orientation-selective responses for a given neuron, and the circular variance of the preferred orientations (see Methods) of all orientation-selective responses of that neuron (Figure 7B, bottom). Agouti orientation-selective V1 neurons exhibit a larger variability in their preferred angles across different SFs than neurons in cat areas 17 and 18.

We then analyzed whether a systematic dependence on SF was present within the observed variability. For this, we computed intra-neuron pairwise angle differences between the orientation-selective responses and classified them according to the distance in SF octaves (Figures 7C and 7D). Here, angle differences from all single units entered which met the selection criteria for at least two SFs of the groups 0.04, 0.08, 0.16, 0.32, and 0.64 cpd (312 agouti, 22 cat A17, and 83 cat A18 single units).

The data for agouti show a displacement toward larger values than cat, as expected from the higher variability discussed above, and also an increase in angle difference as the difference in octaves increases. Cat data, on the other hand, show lower angle difference values than those of agouti for every octave comparison.

Only area 18 (and not 17) appears to show a systematic variation of angle difference with octave difference, although orientation-selective responses of A18 to 0.64 cpd are, as expected from the area 18 SF cutoff, scarce and therefore that data point might not be representative. Pattadkal et al. (2018) have shown that mouse V1 neurons present a shift in the preferred angle with SF. We also found that in our agouti data but not for cat area 17.

Orientation preference maps in agouti

In order to confirm the lack of large-scale periodic orientation columns, we obtained maps of intrinsic signals in three agoutis. Intrinsic signal imaging is known to have a spatial resolution of at least 100 μm

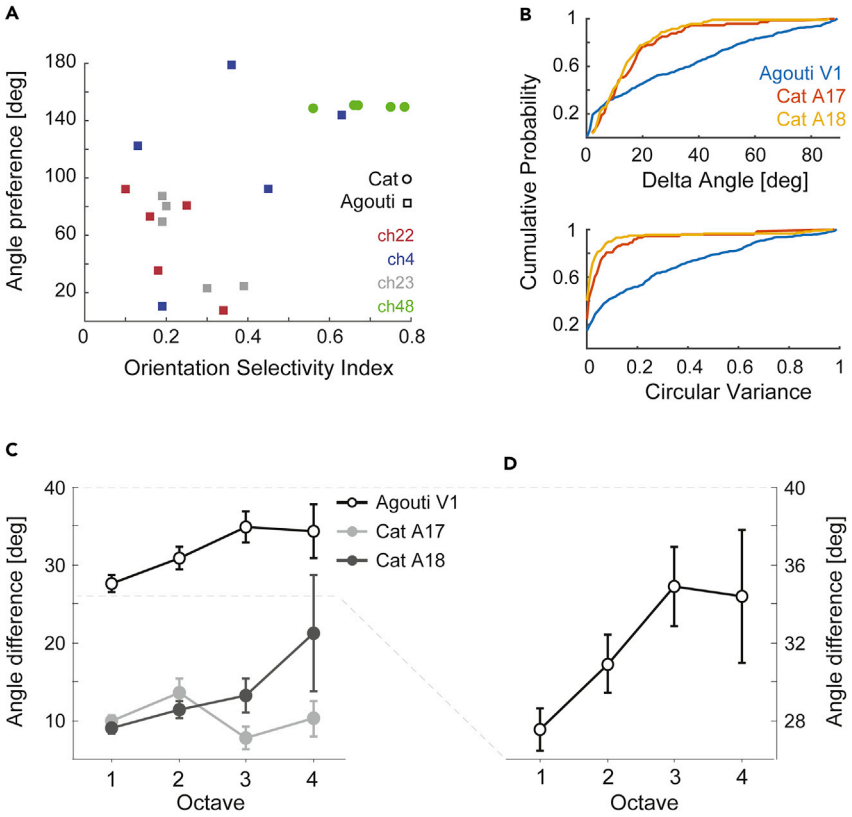

Figure 7. Neuronal (in)stability of preferred angles across different spatial frequencies

(A) Orientation preference and selectivity index at different SFs for three example units from agouti (red, blue, gray squares) and one from cat area 17 (green circles). Note that agouti orientation preference varies much more than the cat's.

(B) Overall cumulative distribution of angle range (top) and circular variance (bottom) for all cells.

(C) Mean of the pairwise within-cell comparisons. For each pair of orientation selective responses (to different spatial frequencies) crossing the selectivity threshold, the difference of preferred angle was computed. The octaves denote the difference in spatial frequencies of the responses being compared (e.g. comparisons between 0.04-0.08 cpd and 0.32–0.64 cpd are both one octave apart).

(D) Zoom into the agouti curve shown in (C). Note that orientation difference increases with SF difference. Error bars: SEM.

(Grinvald et al., 1986). We imaged the field of view exposed lateral to the lateral sulcus during monocular stimulation using two monitor positions of different eccentricity (0–40 deg and 40–80 deg). The checker bar protocol gave rise to specific retinotopic activations in the intrinsic signal maps predicted from Picanço-Diniz et al. (1991, their Figure 1B). According to the movement of the horizontal checker bar from upper to lower visual field, the activation shifted gradually from lateral posterior to medial anterior (Figure 8A). When moving the vertical checker bar in the visual field from medial to lateral, the activation in the single condition maps moved gradually from lateral anterior to medial posterior (Figure 8B). As expected for the enlarged representation of the visual streak, the maps evoked by the central position of the bar (+10 deg until −5 deg) covered together the largest part of the region of interest (yellow-orange-red in the color map). Similar maps were obtained from the other two animals. The landmarks obtained are in concordance with the descriptions of retinotopic maps (Picanço-Diniz et al., 1991; Dias et al., 2014).

Once having successfully obtained intrinsic signals from checker bars, we continued stimulation with gratings of four different orientations (eight directions of motion) and a SF adequate for agouti (0.16 cpd at 2 Hz) on the ideal monitor position.

To avoid any artificial periodicity in the single condition maps by filtering, image subtraction, or cocktail blank normalization, we used only first-frame correction as a preprocessing step. This evoked rather homogeneous activations in the region of interest (ROI) visually stimulated (stimROI). In addition, not all

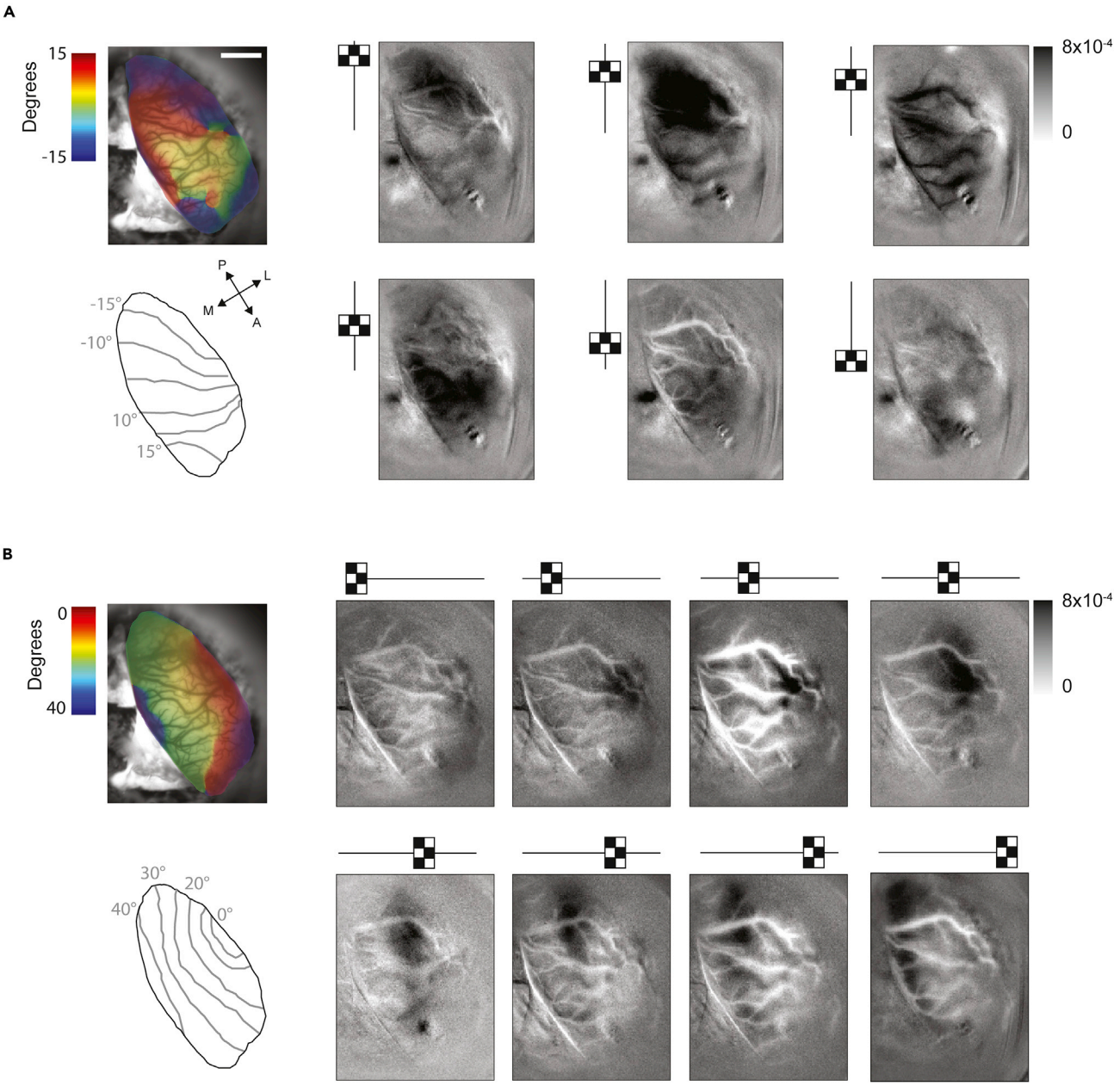

Figure 8. Intrinsic signal maps of retinotopy

Left, upper image: color overlay on the vessel image of position specific activation with bars of 5 deg width spanning the whole monitor in horizontal (A, 6 positions) or vertical (B, 8 positions, indicated by checker sketches on top) orientation. Lower image: sketch depicting iso-elevation (A) or iso-azimuth lines. Right: single condition maps.

(A) The activation starts with 15 deg in the upper visual field activating the lateral-posterior part of the craniotomy migrating to the anterior part. The visual streak extends from red to yellow.

(B) A vertical bar positioned at the visual field's midline evokes activity at anterior-lateral part moving to medial. HM, horizontal meridian; VM, vertical meridian. Cortical coordinates: M, medial; L, lateral; A, anterior; P, posterior.

stimuli were equally efficient in evoking an intrinsic signal. Interestingly, the best activation seemed to be obtained with horizontal gratings. Accordingly, yellow was the dominating color in the compound angle map (Figures 9A and 9B). This finding repeated in all three animals and in both regions of interest along the visual streak representation we obtained per hemisphere/animal (Figure 9C, n = 6). For quantification of the coverage of preferences, orientation preference per pixel after vector summation was

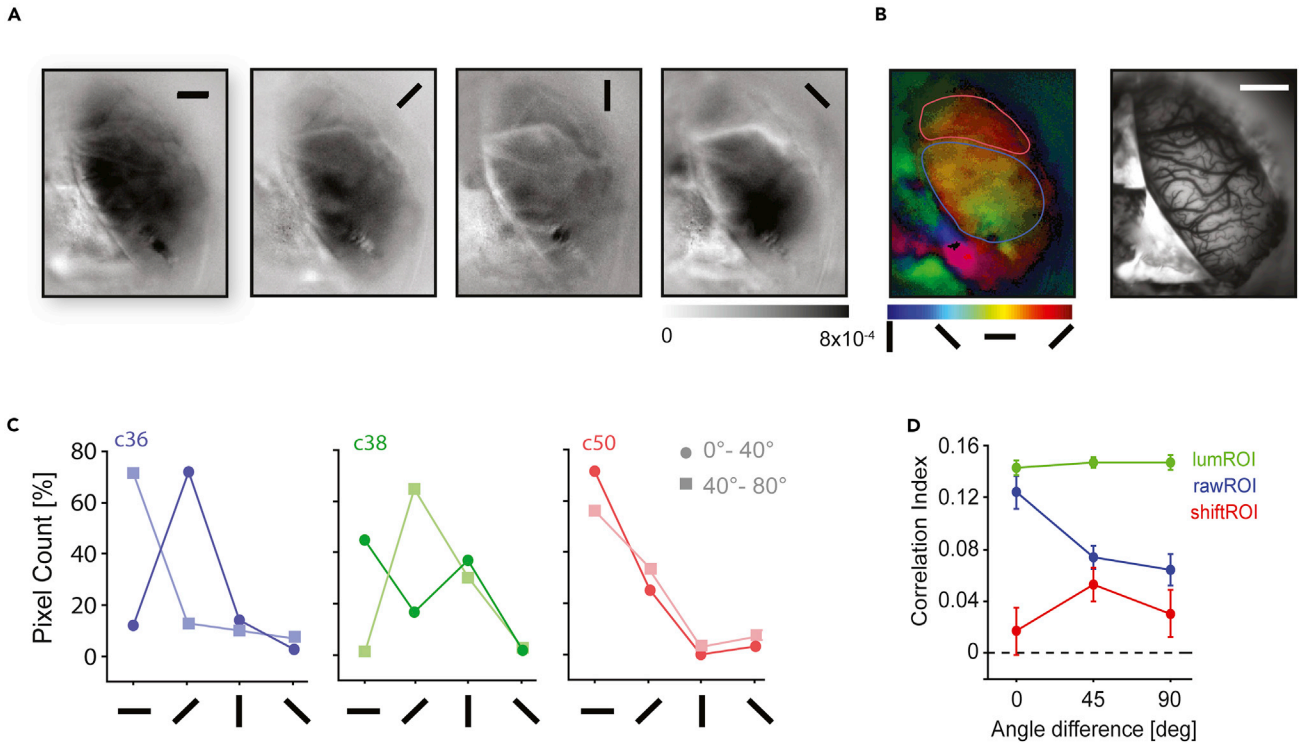

Figure 9. Orientation maps obtained by grating stimulation in agouti primary visual cortex

(A) Unfiltered averaged single condition maps after first frame correction.

(B) Left, polar (saturation of the color codes for vector strength) map according to the color bar below; blue outline, stimROI; red outline, shiftROI. right: vessel image of the recorded area. Scale bar, 1 mm; cortical coordinates as in Figure 8.

(C) Relative count of pixels preferring one of the four angle categories as indicated below in two ROIs, a medial and a more temporal one. Note that preferences for either horizontal or right oblique (recording the left hemisphere) dominate in all animals and ROIs.

(D) Mean spatial correlation coefficients between all frames within the stimulated ROI (blue), an ROI shifted in an area not stimulated by that monitor position (red) and on a rubber brain illuminated with red light (green) for C50. Error bars: SEM.

categorized in four groups of equal size because four different orientations were used for visual stimulation. Confirming the orientation bias observed in the electrophysiological data of single units (Figure 6C), it turned out that indeed the horizontal and/or the right oblique orientation preference dominate in the vector map (Figure 9C).

Since the maps did not present any obvious periodicity or complementarity as known from maps in carnivores and primates, we tested for response reliability to the same stimulus orientation at different moments of the recording session. To this end, we spatially correlated the raw activation values of the first frame corrected pixels in the visually stimulated region of interest (stimROI) of the summed frames per recording block and condition with each other. Correlation values obtained with the same grating at different moments of time were significantly higher than with frames obtained at orthogonal orientations. This was not the case for pixels in a region of interest outside the visually stimulated area (shiftROI) close by (Figure 9D, Mann-Whitney-U test, difference between group 0 vs 90: $n = 2182$, stimROI, $p = 0.0006$; shiftROI, $p = 0.6$). The same result was obtained for the two other animals C36 and C38 (Figure S6).

Since the intrinsic signal is very small, it might reflect overall differences in illumination of the high-contrast whole-field grating on the monitor being reflected into the recording chamber, especially when there is no clear visually evoked signal amplitude. Therefore, we compared correlation values to those obtained from a control recording on a homogeneous rubber surface being exposed to the same illumination and stimulation conditions. As expected for a homogeneous surface, correlation values were higher than in the "real" experiment but homogeneously distributed over all angle differences, thus excluding any systematic influence of that or any other systematic variable (Mann-Whitney-U test, difference between group 0 vs 90: lumROI, $n = 2210$, $p = 0.58$).

DISCUSSION

We characterized orientation- and direction-selective neurons and their spatial layout in the primary visual cortex of agoutis, while recording from multi-electrodes in horizontal or vertical arrangements and obtaining intrinsic signals during stimulation with sinusoidal gratings. In order to relativize our results to a mammal with high orientation selectivity, similar V1 size, and periodic OPMs, we performed the same experiments in cats.

Agouti aCRFs were of small to moderate size throughout the horizontal streak representation. Although neurons exhibited clear orientation and direction preference, selectivity was only half as high as for cats. Neurons responded best at lower SFs (0.08–0.32 cpd), up to 0.64 cpd, with a bias for horizontal contour preference.

Although preferred orientation seems to be similar along the axis perpendicular to the cortical surface, no systematic periodicity was found parallel to it – in contrast to cat area 17 and 18. Optical imaging of intrinsic signals supported these electrophysiological findings, as we observed homogeneous V1 activation by stimulation with oriented gratings.

Receptive fields and spatial acuity

According to our results, agouti aCRFs (1–22 deg^2) can be as small as cat area 17 and 18 fields in the central visual field representation (our own comparison data, and Hubel and Wiesel, 1962). As expected for a rodent, their size does not increase much with eccentricity in the vicinity of the horizontal meridian ($\pm 15^\circ$ elevation), which includes the representation of the agouti's horizontal streak. Previous studies on agouti (Picanço-Diniz et al., 1991) report slightly larger RF sizes of 8–33 deg^2 close to the midline until up to 71 deg^2 in the temporal periphery. The difference might be partially due to our focus on the region close to the horizontal meridian, thus undersampling high/low elevations and far periphery. Further, the automatic algorithm used here delineates aCRFs from the top 30% of the PSTH responses, in contrast to hand mapping taking into account the last spike detected.

Agouti aCRFs are also smaller than those of rats (7–130 deg^2, Girman et al., 1999), much smaller than those of mice (50–700 deg^2, Niell and Stryker, 2008), and appear in the low range of the rabbit's receptive field size (1–60 deg^2, Murphy and Berman, 1979), which – as agouti – is more diurnal than rats and mice (Jilge, 1991).

Thus, our data suggest that agoutis exhibit high visual acuity along their visual streak. Behavioral and visual evoked potential reports indicate an SF cutoff at about 0.6 cpd for mice (Porciatti et al., 1999; Prusky and Douglas, 2004), which is very similar to the cutoff for single unit spiking responses in agoutis. However, multi-unit activity in mice indicates much lower optimal SFs (0.02 cpd, Niell and Stryker, 2008), whereas agouti V1 neurons responded most selectively to 0.32 cpd, about half the cat's optimal SF in V1 (our data; Movshon et al., 1978), and similar to ferrets (Baker et al., 1998).

Orientation and direction selectivity

With the vector summation method, we find highly selective cells in both agouti and cats, but our median values are lower than those reported previously for mice (Niell and Stryker, 2008; Tan et al., 2011) and cats (Gardner et al., 1999; Carandini and Ferster, 2000; Scholl et al., 2013, 2016). When calculating the orthogonal modulation depth index (OMDI), the overall indices rise to the values reported in the previous literature, and, importantly, are highly correlated to the values we used for our further analysis. Moreover, having performed the same experiments in both species allows us to compare agouti and cat selectivity internally, independently of absolute selectivity values. Noteworthy, agoutis tend to have lower firing rates, which might account for reduced OSI values. Thus, we implemented a rate-dependent selectivity index and also compared OSI distribution for rate-matched samples. Still, the remaining data revealed that orientation selectivity in agouti is lower than that in the cat primary visual cortex. Lower selectivity could thus be a consequence of different circuits generating orientation and direction selectivity in the different orders.

Tan et al. (2011) as well as Bopp et al. (2014) found less evidence for lateral inhibition in mouse V1, as opposed to cats. In cortical layouts with modular periodic maps such as primates and carnivores, lateral inhibition might be a crucial mechanism contributing to their high orientation selectivity.

Animals with modular pinwheel-like structures exhibit considerable selectivity in their excitatory long-range connectivity linking preferentially neurons responding to similar orientations and along a similar axis (Schmidt et al., 1997a) (Schmidt et al., 1997b). In contrast, orientation-selective neurons of mice receive inputs that are distributed over a broad range of preferred orientations (Jia et al., 2010); Iacaruso et al., 2017; Lee et al., 2019). Pattadkal et al. (2018) demonstrate that orientation selectivity in rodents lacking orderly maps can emerge from random intracortical connectivity but predict that orientation preference shifts considerably in dependence of SF. In support of the hypothesis that this feature could be common to rodents – and distinct from cats – our data show a clear shift in orientation preference that increases with the difference in stimulated SF also in the big rodent agouti.

Noteworthy, while in carnivores, primates, and rodents, feature selectivity seems to arise from the alignment of geniculo-cortical axons firstly in the cortex (e.g. (Reid and Alonso, 1995; Chapman et al., 1991, (Lien and Scanziani, 2013, 2018; Scholl et al. (2013)) suggest that cortical orientation selectivity in rodents may also be directly adopted from orientation-selective neurons in the lateral geniculate nucleus.

Functional layout

Pinwheel-like OPMs are present in all primates and carnivores studied so far. In contrast, rodents and lagomorphs (Van Hooser, 2007) show an interspersed organization of orientation selective neurons in their visual cortices. Although this suggested phylogeny as a main reason for the observed differences, theoretical studies proposed that a small V1 size could be an alternative reason for the lack of OPMs (Meng et al., 2012) and that it may put constrains on map structure (Keil et al., 2012). The agouti has the largest rodent V1 studied so far. Accordingly, Weigand et al. (2017), from simulations of a transition from interspersed to periodic OPMs and its dependence on the number of interconnected neurons, suggested that agoutis (and capybara) "likely possess OPMs".

Contrary to this theoretical prediction, our results do not support the presence of periodic orientation preference maps in agouti V1. Although we cannot rule out the possibility of orientation maps with a periodicity smaller than 250 um, due to our electrode spacing, such periodicity (with its implied pinwheel density) is unexpected for a visual cortex the size of the agouti's (Kaschube et al., 2010). Interestingly, in agreement with an absence of modularity, the agouti visual cortex also lacks CO blobs (Dias et al., 2014).

Arguing against the hypothesis of a uniform mechanism constrained by brain size is also a recent report of pinwheels and OPMs in mouse lemur V1, the smallest primate studied so far (Ho et al., 2020).

To be further noted, agoutis – as other rodents – have been reported to possess lower neuronal densities than species with OPMs (review in Weigand et al., 2017; personal communication, M. Garcia), which opens the possibility that although absolute size does not matter, density of neurons might. Lower densities of striate neurons could go along with lower density of thalamo-cortical afferents and maybe absent clustering of ON/OFF responses, which is held responsible for spatially ordering cortical neurons in carnivores and primates (Kremkow et al., 2016; Kremkow and Alonso, 2018).

Yet, not all neural densities of the investigated species are firmly known, and theoretical considerations speak against neuronal density as a major factor (Ibbotson and Jung, 2020). More characteristics of rodents are laterally positioned eyes and a low central-peripheral density ratio of retinal ganglion cells due to the absence of a fovea. Thus, Ibbotson and Jung (2020) discuss that the central-peripheral ratio is more closely associated than neuronal density with the expression of pinwheel-like structures predicting an interspersed layout for big rodents such as agoutis.

Alternative ideas – independent of brain size or neuron density – posit rodent-specific connectivity influencing the excitation-inhibition balance (Ohki and Reid, 2007; Hansel and van Vresswjik, 2012; Sadeh and Rotter, 2015) or the extent of astrocyte arbors of restricting the size of hypercolumns (Philips et al., 2017) as responsible for the lack of columns in rodents. Given the low selectivity and the lack of large-scale periodicity of orientation preference in agoutis, our results are consistent with these models.

Nevertheless, it is important to note that interspersed does not necessarily equal random organization. Recent studies have indicated that a "mini-columnar" structure of iso-oriented cells is present in mice (Ringach et al., 2016; Scholl et al., 2016; Kondo et al., 2016; Maruoka et al., 2017). Our results are consistent

with this organizational structure since neurons recorded from the same site or along the axis perpendicular to the cortical surface tend to be more similar than neurons recorded parallel to it. However, mouse "mini-columns" have a radius of less than 50 μm, measured via 2-photon imaging at a high resolution (Ringach et al., 2016; Kondo et al., 2016). Such a periodicity would escape the resolution of intrinsic signal imaging and also electrophysiological recordings from 1 MΩ electrodes that sample from a radius of about 50–100 μm around their tip (Henze et al., 2000), rendering it impossible to assert if the local structure we see in agoutis reflects the same feature. Moreover, the similarity of orientation preference along the vertical axis could be partially explained by the pronounced orientation anisotropy for horizontal preference in our data. On the other hand, an evenly distributed orientation bias would be expected to shift differences toward smaller orientation preference differences also in the horizontal cortical axis. Since these differences are increasing more rapidly with distance in the horizontal than in the vertical axis, our data essentially favor a "mini-columnar" organization.

It would be important to include the orientation anisotropy into models of the visual cortical layout because it seems to be a feature common to species with a visual streak and low central-periphery ratio (rats: Girman et al., 1999; mouse: Dräger 1975; Salinas et al., 2017; hamster: Tiao and Blakemore 1976 and rabbits: Bousfield 1977; Murphy and Berman, 1979) and could be inherited from a bias in the retino-geniculo-cortical input.

In conclusion, our data fill an important gap of knowledge about cortical evolution as they support that phylogenetic trait – including a specific retinal layout – is more predictive for formation of periodic orientation maps than brain size. Future studies should elucidate the agoutis' functional layout on the cellular level and its local circuits producing feature selectivity.

Limitations of the study

It should be noted that the smallest available distance between simultaneously recorded channels in the horizontal axis was 250 μm and in the vertical axis 100 μm. This limits the resolution of angle differences in space and thus our conclusion pointing toward units preferring similar orientation preference clustering together. However, the observation that single units isolated from the same multi-unit (0 μm angle difference) frequently had more similar orientation preference supports that our data are in agreement with a not entirely random organization, i.e., with the previously observed mini-columns in rodents.

Resource Availability

Lead Contact

Further information and requests for resources should be directed to and will be fulfilled by the Lead Contact, Kerstin Schmidt (kschmidt@neuro.ufrn.br).

Material Availability

This study did not generate new unique reagents. The original datasets from the agouti species have not been deposited in a public repository yet.

Data and Code Availability

Data and codes that support the findings of this study are available from the authors upon reasonable request.

METHODS

All methods can be found in the accompanying Transparent Methods supplemental file.

SUPPLEMENTAL INFORMATION

Supplemental Information can be found online at https://doi.org/10.1016/j.isci.2020.101882.

ACKNOWLEDGMENTS

This work was supported by Coordenação de Aperfeiçoamento de Pessoal de Nível Superior (CAPES), Conselho Nacional de Desenvolvimento Tecnológico (CNPq), by the VW Foundation (ZN2632), BCCN (01GQ1005A and 01GQ1005B), DFG (CRC 1286, 889; SPP 2205), the Ministry for Science and Culture of

Lower Saxony, and the Max Planck Society. We are grateful to S. Neuenschwander for the SPASS acquisition/MEC stimulation system and the NES tool to T. Wunderle for the OIAnalyzer, and to W. Dantas for excellent animal care.

AUTHOR CONTRIBUTIONS

Conceptualization, K.E.S. and F.W.; Methodology, K.E.S., D.N.F., and S.C.O., Investigation, K.E.S., D.N.F., S.C.O., J.H.N.P., and L.C.S.; Writing – Original Draft, D.N.F. and K.E.S.; Writing – Review & Editing, K.E.S., F.W., and S.C.O.; Funding Acquisition, K.E.S.; Resources, M.O.; Supervision, K.E.S.

DECLARATION OF INTERESTS

The authors declare no competing interests.

Received: April 23, 2020
Revised: October 16, 2020
Accepted: November 25, 2020
Published: January 22, 2021

REFERENCES

Bachatene, L., Bharmauria, V., Cattan, S., Chanauria, N., Etindele-Sosso, F.A., and Molotchnikoff, S. (2016). Functional synchrony and stimulus selectivity of visual cortical units: comparison between cats and mice. Neuroscience *337*, 331–338.

Baker, G.E., Thompson, I., Krug, K., Smyth, D., and Tolhurst, D.J. (1998). Spatial-frequency tuning and geniculocortical projections in the visual cortex (areas 17 and 18) of the pigmented ferret. Eur. J. Neurosci. https://doi.org/10.1046/j.1460-9568.1998.00276.x.

Blasdel, G.G., and Salama, G. (1986). Voltage-sensitive dyes reveal a modular orgnaization in monkey striate cortex. Nature *321*, 579–585.

Bonhoeffer, T., and Grinvald, A. (1991). Iso-orientation domains in cat visual cortex are arranged in pinwheel-like patterns. Nature *353*, 429–431.

Bonin, V., Histed, M.H., Yurgenson, S., and Reid, R.C. (2011). Local diversity and fine-scale organization of receptive fields in mouse visual cortex. J. Neurosci. *31*, 18506–18521.

Bopp, R., Macarico da Costa, N., Kampa, B.M., Martin, K.A.C., and Roth, M.M. (2014). Pyramidal cells make specific connections onto smooth (GABAergic) neurons in mouse visual cortex. PLoS Biol. *12*, e1001932, https://doi.org/10.1371/journal.pbio.1001932.

Bousfield, J.D. (1977). Columnar organization and the visual cortex of the rabbit. Brain Res. *136*, 154–158.

Carandini, M., and Ferster, D. (2000). Membrane potential and firing rate in cat primary visual cortex. J. Neurosci. *20*, 470–484.

Chapman, B., Zahs, K.R., and Stryker, M.P. (1991). Relation of cortical cell orientation selectivity to alignment of receptive fields of the geniculocortical afferents that arborize within a single orientation column in ferret visual cortex. J. Neurosci. *11*, 1347–1358.

Chapman, B., Stryker, M.P., and Bonhoeffer, T. (1996). Development of orientation preference maps in ferret primary visual cortex. J. Neurosci. *16*, 6443–6453.

Chklovskii, D.B., and Koulakov, A.A. (2004). Maps in the brain: what can we learn from them? Annu. Rev. Neurosci. *27*, 369–392.

Conde-Ocazionez, S.A., Jungen, C., Wunderle, T., Eriksson, D., Neuenschwander, N., and Schmidt, K.E. (2018). Callosal influence on visual receptive fields has an ocular, an orientation-and direction bias. Front. Syst. Neurosci. *12*, 1–13.

Dias, I., Bahia, C.P., Franca, J.G., Houzel, J.C., Lent, R., Mayer, A.O., Santiago, L.F., Silveira, L.C., Picanço-Diniz, C.W., and Pereira, A. (2014). Topography and architecture of visual and somatosensory areas of the agouti. J. Comp. Neurol. *522*, 2576–2593.

Dräger, U.C. (1975). Receptive fields of single cells and topography in mouse visual cortex. J. Comp. Neurol. *160*, 269–290.

Essen, D., and Zeki, S. (1978). The topographic organization of Rhesus monkey prestriate cortex. J. Physiol. *277*, 193–226.

Gardner, J.L., Anzai, A., Ohzawa, I., and Freeman, R.D. (1999). Linear and nonlinear contributions to orientation tuning of simple cells in the cat's striate cortex. Vis. Neurosci. *16*, 1115–1121.

Girman, S.V., Sauvé, Y., and Lund, R.D. (1999). Receptive field properties of single neurons in rat primary visual cortex. J. Neurophysiol. *82*, 301–311.

Grinvald, A., Lieke, E., Frostig, R.D., Gilbert, C.D., and Wiesel, T. (1986). Functional architecture of cortex revealed by optical imaging of intrinsic signals. Nature. https://doi.org/10.1038/324361a0.

Hansel, D., and van Vresswjik, C. (2012). The mechanism of orientation selectivity in primary visual cortex without a functional map. J Neurosci. https://doi.org/10.1523/JNEUROSCI.6284-11.2012.

Hebb, D.O. (1949). The Organization of Behavior (Wiley).

Henze, D.A., Borhegyi, Z., Csicsvari, J., Mamiya, A., Harris, K.D., and Buzsáki, G.J. (2000). Intracellular features predicted by extracellular recordings in the hippocampus in vivo. J. Neurophysiol. *84*, 390–400.

Ho, C.L.A., Zimmermann, R., Flórez Weidinger, J.D., Prsa, M., Schottdorf, M., Merlin, S., Okamoto, T., Ikezoe, K., Pifferi, F., Aujard, F., et al. (2020). Orientation preference maps in Microcebus murinus reveal size-invariant design principles in primate visual cortex. Curr. Biol. https://doi.org/10.1016/j.cub.2020.11.027, 03.12.20.

Hubel, D.H., and Wiesel, T. (1965). Receptive Fields and Functional Architecture in two Nonstriate Visual Areas (18 and 19) of the Cat. J Neurophysiol. https://doi.org/10.1152/jn.1965.28.2.229.

Hubel, D.H., and Wiesel, T.N. (1968). Receptive fields and functional architecture of monkey striate cortex. J. Physiol. *195*, 215–243.

Hubel, D.H., and Wiesel, T.N. (1963). Receptive fields of cells in striate cortex of very young, visually inexperienced kittens. J. Neurophysiol. *26*, 994–1002.

Hubel, D.H., and Wiesel, T.N. (1962). Receptive fields, binocular interaction and functional architecture in the catś visual cortex. J. Physiol. *160*, 106–154.

Iacaruso, M.F., Gasler, I.T., and Hofer, S.B. (2017). Synaptic organization of visual space in primary visual cortex. Nature *547*, 449–452.

Ibbotson, M., and Jung, Y.J. (2020). Origins of functional organization in the visual cortex. Front. Syst. Neurosci. *14*, 1–13.

Jia, H., Rochefort, N.L., Chen, X., and Konnerth, A. (2010). Dendritic organization of sensory input to cortical neurons in vivo. Nature. https://doi.org/10.1038/nature08947.

Jilge, B. (1991). The rabbit: a diurnal or a nocturnal animal? J. Exp. Anim. Sci. *34*, 170–183.

Jones, J.P., Stepnoski, A., and Palmer, L.A. (1987). The two-dimensional spectral structure of simple receptive fields in cat striate cortex. J. Neuropysiol. *58*, 1214–1232.

Kaschube, M., Schnabel, M., Löwel, S., Coppola, D.M., White, L.E., and Wolf, F. (2010). Universality in the evolution of orientation columns in the visual cortex. Science *330*, 1113–1116.

Keil, W., Kaschube, M., Schnabel, M., Löwel, S., Coppola, D.M., White, L.E., and Wolf, F. (2012). Response to comment on "Universality in the evolution of orientation columns in the visual cortex. Science *330*, 1113–1116.

Kondo, S., Yoshida, T., and Ohki, K. (2016). Mixed functional microarchitectures for orientation selectivity in the mouse primary visual cortex. Nat. Commun. *7*, 13210.

Koulakov, A.A., and Chklovskii, D.B. (2001). Orientation preference patterns in mammalian visual cortex: a wire length minimization approach. Neuron *29*, 519–527.

Kremkow, J., and Alonso, J.-M. (2018). Thalamococortical circuits and functional architecture. Annu. Rev. Vis. Sci. *4*, 263–285.

Kremkow, J., Jin, J., Wang, Y., and Alonso, J.-M. (2016). Principles underlying sensory map topography in primary visual cortex. Nature *533*, 52–57.

Lee, K.S., Vandemark, K., Mezey, D., Shultz, N., and Fitzpatrick, D. (2019). Functional synaptic architecture of callosal inputs in mouse primary visual cortex. Neuron *101*, 421–428.

Lien, A.D., and Scanziani, M. (2013). Tuned thalamic excitation is amplified by visual cortical circuits. Nature Neurosci. https://doi.org/10.1038/nn.3488.

Lien, A.D., and Scanziani, M. (2018). Cortical direction selectivity emerges at convergence of thalamic synapses. Nature *558*, 80–86.

Löwel, S., and Singer, W. (1992). Selection of intrinsic horizontal connections in the visual cortex by correlated neuronal activity. Science *255*, 209–212.

Löwel, S., Freeman, B., and Singer, W. (1987). Topographic organization of the orientation column system in large flatmounts of the cat visual cortex: a 2 deoxyglucose study. J. Comp. Neurol. *255*, 401–415.

Maruoka, H., Nagakawa, N., Tsuruno, S., Sakai, S., Yoneda, T., and 1Hosoya. (2017). Lattice system of functionally distinct cell types in the neocortex. Science *358*, 610–615.

Mazurek, M., Kager, M., and Van Hooser, S.D. (2014). Robust quantification of orientation selectivity and direction selectivity. Front. Neural Circuits *8*, 92, https://doi.org/10.3389/fncir.2014.00092. eCollection 2014.

Meng, Y., Tanaka, S., and Poon, C.-S. (2012). Comment on "universality in the evolution of orientation columns in the visual cortex". Science *336*, 413.

Movshon, J.A., Thompson, I.D., and Tolhurst, D.J. (1978). Spatial and temporal contrast sensitivity of neurones in arwas 17 and 18 of the cat's visual cortex. J. Opt. Soc. Am. *283*, 101–120.

Murphy, E.H., and Berman, N. (1979). The rabbit and the cat: a comparison of some features of response properties of single cells in the primary visual cortex. J. Comp. Neurol. *188*, 401–428.

Niell, C.M., and Stryker, M.P. (2008). Highly selective receptive fields in mouse visual cortex. J. Neurosci. *28*, 7520–7536.

Ohki, K., Chung, S., Ch'ng, Y.H., Kara, P., and Reid, R.C. (2005). Functional imaging with cellular resolution reveals precise micro-architecture in visual cortex. Nature *433*, 597–603.

Ohki, K., and Reid, R.C. (2007). Specificity and randomness in the visual cortex. Curr Opin Neurobiol. https://doi.org/10.1016/j.conb.2007.07.007.

Orban, G.A., Kennedy, H., and Maes, H. (1981). Response to movement of neurons in areas 17 and 18 of the cat: direction selectivity. J. Neurophysiol. *45*, 1059–1073.

Pattadkal, J.J., Mato, G., van Vreeswijk, C., Priebe, N.J., and Hansel, D. (2018). Emergent orientation selectivity from random networks in mouse visual cortex. Cell Rep. *24*, 2042–2050.

Peiker, C., Wunderle, T., Eriksson, D., Schmidt, A., and Schmidt, K.E. (2013). An updated midline rule: visual callosal connections anticipate shape and motion in ongoing activity across the hemispheres. J. Neurosci. *33*, 18036–18046.

Philips, R.T., Sur, M., and Chakravarthy, V.S. (2017). The influence of astrocytes on the width of orientation hypercolumns in visual cortex: a computational perspective. PLoS Comput. Biol. *13*, e1005785.

Picanço-Diniz, C.W., Silveira, L.C.L., De Carvalho, M.S.P., and Oswaldo-Cruz, E. (1991). Contralateral visual field representation in area 17 of the cerebral cortex of the agouti: a comparison between the cortical magnification factor and retinal ganglion cell distribution. Neuroscience *44*, 325–333.

Porciatti, V., Pizzorusso, T., and Maffei, L. (1999). The visual physiology of the wild type mouse determined with pattern VEPs. Vis. Res. *39*, 3071–3081.

Prusky, G.T., and Douglas, R.M. (2004). Characterization of mouse cortical spatial vision. Vis. Res. *44*, 3411–3418.

Reid, R.C., and Alonso, J.M. (1995). Specificity of monosynaptic connections from thalamus to visual cortex. Nature. https://doi.org/10.1038/378281a0.

Ribot, J., Aushana, Y., Bui-Quoc, E., and Milleret, C. (2013). Organization and origin of spatial frequency maps in cat visual cortex. J. Neurosci. *33*, 13326–13343.

Ringach, D.L., Mineault, P.J., Tring, E., Olivas, N.D., Garcia-Junco-Clemente, P., and Trachtenberg, J.T. (2016). Spatial clustering of tuning in mouse primary visual cortex. Nat. Commun. *7*, 12270.

Sadeh, S., and Rotter, S. (2015). Orientation selectivity in inhibition-dominated networks of spiking neurons: effect of single neuron properties and network dynamics. PLOS Computational Biol. https://doi.org/10.1371/journal.pcbi.1004045.

Salinas, K.J., Figueroa Velez, D.X., Zeitoun, J.H., Kim, H., and Gandhi, S.P. (2017). Contralateral bias of high spatial frequency tuning and cardinal direction selectivity in mouse visual cortex. J. Neurosci. *37*, 10125–10138.

Schmidt, K.E., Goebel, R., Löwel, S., and Singer, W. (1997b). The perceptual grouping criterion of colinearity is reflected by anisotropies of connections in the primary visual cortex. Eur J Neurosci. https://doi.org/10.1111/j.1460-9568.1997.tb01459.x.

Schmidt, K.E., Kim, D.-S., Singer, W., Bonhoeffer, T., and Löwel, S. (1997a). Functional specificity of long-range intrinsic and interhemispheric connections in the visual cortex of strabismic cats. J Neurosci. https://doi.org/10.1523/JNEUROSCI.17-14-05480.1997.

Scholl, B., Pattadkal, J.J., Rowe, A., and Priebe, N.J. (2016). Functional characterization and spatial clustering of visual cortical neurons in the predatory grasshopper mouse Onychomys arenicola. J. Neurophysiol. https://doi.org/10.1152/jn.00779.2016.

Scholl, B., Tan, A.Y.Y., Corey, J., and Priebe, N.J. (2013). Emergence of orientation selectivity in the Mammalian visual pathway. J. Neurosci. *33*, 10616–10624.

Tan, A.Y.Y., Brown, B.D., Scholl, B., Mohanty, D., and Priebe, N.J. (2011). Orientation selectivity of synaptic input to neurons in mouse and cat primary visual cortex. J. Neurosci. *31*, 12339–12350.

Tiao, Y.C., and Blakemore, C. (1976). Functional organiztaion in the visual cortex oft he golden hamster. J. Comp. Neurol. *168*, 459–482.

Ts'o, D.Y., Frostig, R.D., Lieke, E.E., and Grinvald, A. (1990). Functional organization of primate visual cortex revealed by high resolution optical imaging. Science *249*, 417–420.

Van Hooser, S.D. (2007). Similarity and diversity in visual cortex: is there a unifying theory of cortical computation? Neuroscientist *13*, 639–656.

Van Hooser, S.D., Heimel, J.A., and Nelson, S.B. (2005). Functional cell classes and functional architecture in the early visual system of a highly visual rodent. Prog. Brain Res. *149*, 127–145.

Weigand, M., Sartori, F., and Cuntz, H. (2017). Universal transition from unstructured to structured neural maps. Proc. Natl. Acad. Sci. U S A *114*, E4057–E4064.

Wolf, F., and Geisel, T. (1998). Spontaneous pinwheel annihilation during visual development. Nature *398*, 326–330.

Wunderle, T., Eriksson, D., and Schmidt, K.E. (2013). Multiplicative mechanism of lateral interactions revealed by controlling interhemispheric input. Cereb. Cortex *23*, 900–912.

iScience, Volume *24*

Supplemental Information

Spatial clustering of orientation preference in primary visual cortex of the large rodent agouti

Dardo N. Ferreiro, Sergio A. Conde-Ocazionez, João H.N. Patriota, Luã C. Souza, Moacir F. Oliveira, Fred Wolf, and Kerstin E. Schmidt

Transparent methods

Experiments were performed at the Brain Institute of the Federal University of Rio Grande do Norte (UFRN), Brazil, in twelve adult female agoutis (1-2 years) bred at the Universidade Federal Rural do Semi-Árido (UFERSA) and five adult female cats (1-3 years) bred at the Brain Institute's colony. The study was carried out in accordance with the recommendations of the Society for Neuroscience, the Brazilian Law for the Protection of Animals and in accordance with the conservation regulation of biodiversity in Brazil (SISBio, protocol number: 53756). The experimental protocols were approved by the Ethical Committee for the Use of Animals of the University of Rio Grande do Norte in Natal (CEUA, protocol number: 006/2013), Centro de Biociências, UFRN.

Anesthesia and surgical procedures

Anesthesia was induced by intramuscular injection of a mixture of 40 mg/kg of ketamine (Quetamina, Vetecia LTDA, Brazil) and 10 mg/kg of xylazine hydrochloride (Virbaxyl, Rhobifarma LTDA, Brazil) for agoutis, and 20 mg/kg of ketamine and 2 mg/kg of xylazine for cats. All animals (of both species) also received 0.1 mg/kg of atropine (Atropine sulphate, Atrofarma, Brazil). In order to prevent inflammation, a daily dose of 0.1 mg/kg of dexamethasone (Cortiflan, Ourofino, Brazil) was administered intravenously. After tracheostomy, we maintained anesthesia with isoflurane (for ten agoutis), or halothane (for all cats and two agoutis) and a mixture of N_2O/O_2 (70/30%). The vaporized anesthetic concentration was maintained between 1-2% (for isoflurane) and 1-1.5% (for halothane) throughout the surgery, and lowered to 0.8 % (for isoflurane) and 0.6% (for halothane) during the recordings. Body temperature, inspiratory pressure, electrocardiogram and exhaled CO_2 levels were monitored continuously throughout the experiments.

In order to control for involuntary eye movements, after completion of all surgical procedures, and throughout the experiment, the animals were paralyzed by an initial intravenous bolus of 0.6 mg/kg for cats and 0.3 mg/kg for agoutis of pancuronium bromide (Pancuron, Cristália, Brazil), followed by continuous intravenous infusion of 0.15 mg/kg/hr for cats and 0.10 mg/kg/hr for agoutis of the same drug.

In eleven agoutis, we performed electrophysiology. In two of these eleven animals, electrophysiology was performed after completing optical imaging, and in a third animal only optical imaging of intrinsic signals was obtained.

Optical imaging of intrinsic signals

For intrinsic signal imaging, we performed an oval craniotomy (10 mm x 4.5 mm in the main axes) centered over Horsley-Clarke coordinates AP 11, ML +5 on the left lateral cortex (tentorial surface). A recording chamber was secured with dental cement and, after removal of the dura, filled with silicon oil for intrinsic signal imaging. A surface image was obtained with green illumination (560 nm), and subsequently the camera was focused 600 µm below the pial surface. Functional frames were acquired while illuminating with light of a wavelength of 620 nm with a 12 mm CCD camera (Dalsa 1M60) through a macroscope fitted with an 1x objective (Imager 3001, Optical Imaging Inc, New York (USA). Rate of acquisition was 5 Hz and resolution 512x512.

Electrophysiological recordings

We opened one rectangular lateral craniotomy of about 6.5 x 3 mm centered on Horsley-Clarke coordinates AP 11, ML +5 in the remaining nine agoutis (which didn't undergo optical imaging recordings), and of 8 x 6 mm centered on Horsley-Clarke coordinates AP 0 to -2, ML +2 in five cats. In all agoutis, we recorded from the left hemisphere except one where we obtained data from both visual cortices.

Two types of electrodes were used, although never combining the different types within the same individual animal. From here on, we will refer to the two types of electrodes as 'arrays' or 'probes'. Either up to 3 microelectrode 'arrays' (4 x 4, spacing 250 or 400 µm, 1MΩ, 50 µm diameter, Microprobes, Gaithersburg, MA, USA), or one 'probe' containing two shanks of 16 recording sites each, arranged vertically (500 µm shank spacing, 100 µm spacing between adjacent recording sites, NeuroNexus, Ann Arbor, MI, USA) were lowered into the cortex. In agoutis, we followed anatomical landmarks given in the retinotopic maps of Dias et al. (2014) and Picanço-Diniz et al. (1991) to enhance sampling of receptive fields around the horizontal streak. In cats, we aimed to record from both areas 17 and 18 close to the horizontal meridian representation. After electrode insertion and confirmation of visual responses, agarose solution (3-5% in 0.9% NaCl) was placed over the craniotomy to prevent desiccation and reduce pulsations. Extra-cellular multi-unit activity and local field potentials were recorded using Plexon amplifiers (Plexon Inc., Dallas, TX, USA). For multi-unit activity, signals were amplified 1000 fold, high pass filtered (0.7–6 kHz), thresholded manually around 4 standard deviations well above noise level, digitized with M-series acquisition boards (National Instruments, USA) and stored by a custom-made program in LabView (SPASS by S. Neuenschwander).

Visual stimulation

Eyes were treated with drops of atropine sulfate 1% (Allergan Inc., Brazil) and neosynephrine 1% (Ursapharm, Germany), in order to dilate the pupils and retract the nictitating membrane. Eye refraction was measured with a Rodenstock refractometer and appropriate correcting contact lenses with an artificial pupil of 3 mm were applied in order to refract the optical apparatus to approximately -1.5 diopters. For agoutis, lenses with a diameter of 10 mm and a radius of 6.55 mm, and for cats, lenses with a diameter of 15 mm and a radius of 8.5 mm were used. The animals were secured with a head holder enabling rotation of the head. In both cat and agouti, the sagittal plane through the animal's nose was estimated to match the vertical midline of the visual field. As in Picanço-Diniz et al. (1991), in agouti, the palpebral cleft was used as landmark for the horizontal meridian, which corresponds to the visual streak (Silveira et al., 1989). In cats, the positions of fovea and optic disc were projected with a fundus camera.

Stimuli were presented on a 21'' CRT monitor placed at 57 cm in front of the animals' eyes. This rendered a stimulation area of 30 x 40 degrees of the visual field. The monitor could be moved on an arc at 57 cm distance rendering stimulus positions of up to 120 degrees laterally. Stimulus presentation was controlled using custom software in LabView (MEC by S. Neuenschwander).

For electrophysiology, two types of whole-field stimulation were presented during the experiments. Firstly, since the visual field to be covered simultaneously was considerably large and recording time limited, we opted for an efficient 2D mapping method of receptive fields (Fiorani et al., 2014). To this end, drifting bars moving in 16 different directions (22.5º steps) with a width of 1º and a speed of 20º/s for 2000 ms were used. This particular stimulus was also adequate because a majority of units we encountered in the agouti were of complex type (following the classification of Skottun et al., 1991; data not shown).
Secondly, in order to characterize receptive field properties, sine wave gratings moving in 12 different directions of 30º steps, 7 spatial frequencies of 0.04, 0.08, 0.16, 0.32, 0.64, 1,28 and 2,56 cycles/degree (cpd) and three temporal frequencies of 2, 4 and 8 Hz were presented. Trials with gratings consisted of 500 ms of pre-stimulus activity recording during which an isoluminant grey screen was presented on the monitor, followed by 2000 ms of stimulus presentation. Each stimulus condition was repeated at least 15 times in a pseudo-randomized order. In two of the cats, we used the SFs 0.15, 0.5 and 0.1 cpd. These cats were not included in the analyses comparing different SFs (Figs 2, 3 and 7).
Agoutis, due to their laterally positioned eyes, were stimulated monocularly (contralaterally to the recorded hemisphere), cats were stimulated binocularly after having their eyes aligned with an optic prism.

For optical imaging of retinotopy, we used a set of 14 checkerboard bars of 5 deg spanning the monitor either vertically (8 conditions) or horizontally (6 conditions). Checker bars were filled with 2.5x2.5 deg squares flickering between black and white at 2Hz and were presented for 9000 ms and frames were recorded during the entire stimulus presentation (45 frames of 200 ms duration).
For functional imaging of orientation selective responses, whole-field square-wave gratings moving in eight different directions at a spatial frequency 0.16 cpd and a temporal frequency of 2 Hz were presented for 3000 ms while 15 frames of 200 ms duration were recorded. We tested different spatial frequencies but vector strengths tended to be strongest at that stimulation. For both stimulus types, the inter-stimulus interval was 7000 ms, each condition was repeated 20-30 times and presented in a pseudo-random manner during 10-15 presentation blocks (binning of two frames).

Data Analysis

Electrophysiology

All electrophysiological data were processed using Matlab (R2014b, Mathworks) custom made codes to read, organize, select and analyze the recorded data. In order to obtain single unit time stamps, we applied WaveClus, a spike sorting toolbox, which calculates a set of parameters based on wavelet decomposition of spike waveforms, followed by a super-paramagnetic clustering (for details see Quiroga et al., 2004). Only those single units that showed a significantly higher spiking activity to the stimulus than to the pre-stimulus period of the trials (Sign test, $p < 0.05$) were included in further analysis.
For illustrations, we extracted single waveforms with the NES tool (by S. Neuenschwander, Labview, NI).

Receptive Field Area

Since spike rates of agouti were rather low, we used aggregate classical receptive fields (aCRF) of multi-unit activity in order to increase the sensitivity in determining the RF center and size of our 2D mappings, instead of mapping single units individually. A second reason was to be able to compare our results to previous studies with hand-held stimuli in the agouti.
A peri-stimulus time histogram (PSTH) of the multi-unit spiking response to the drifting bar was created (width = 1º, length = 30º, speed = 20º/s) using a Gaussian smoothing kernel with a SD of 12.7 ms for each of the 16 mappings. Then, each PSTH was normalized to its maximum height in order to weight each stimulus direction equally. Subsequently, PSTHs for a certain channel were projected to the visual mapping field and summed across stimulus directions. The resulting response density maps were

additionally low pass filtered (2D Gaussian smoothing with a SD of 5.88º) and the receptive field was defined as the area above 70% of the maximal response. For each receptive field map, a pair-wise distance between pixels above threshold was computed. The distribution of mean and standard deviation values from all recording sites per animal was calculated. Intuitively, receptive fields map candidates with physiologically based mean and low standard deviation values were associated to well-defined receptive fields. Thus, statistical thresholds for these parameters were established to select recording sites for further analysis (for details see Conde-Ocazionez et al., 2018 and also Fig. S2).

Orientation and Direction Tuning

Orientation and direction preference were defined by an angle and a selectivity index (SI). The selectivity index was calculated by equation 1, i.e. by vectorial summation of spike counts across all trials and stimulus orientations or directions,

$$Selectivity\ Index\ = \frac{\sqrt{(\sum R(\theta_i)\ |cos\ (\theta_i)|)^2 + \sum R(\theta_i)\ |sin(\theta_i)|)^2}}{\sum R(\theta_i)} \quad \text{eq. 1}$$

where *Selectivity Index* can be an orientation selectivity index (OSI) or a direction selectivity index (DSI). $R(\theta_i)$ is a vector with magnitude equal to the accumulated spike count as response to condition *i* across all repetitions and angle defined by θ. The SI ranges between 0 and 1 considering the former as no tuning, where the unit has exactly the same response (if any) to all conditions and the latter as the perfectly selective tuning where the unit responds only to a single condition. The angle of the SI resulting vector corresponds to the preferred angle of the unit.

For calculations of direction tuning, the twelve directions of movement present in our drifting grating stimuli were used. For orientation tuning, the responses to parallel directions of movement were summed (e.g. response to 0º + response to 180º), resulting in six stimulus orientations.

In previous cat experiments (Wunderle et al., 2013; Peiker et al., 2013; Conde-Ocazionez et al., 2018), a fixed threshold of 0.2 for the tuning index defined the subsample of selective units considered for further analysis. Although this value serves well for recordings in cats, the threshold might be inappropriate when studying species/cells that present low firing rates (Mazurek et al., 2014).

Agouti recordings presented lower firing rates than cats, making it more likely to get a high selectivity index simply by sporadic spontaneous activity. In order to minimize false positives, we applied a simple method to adjust the threshold depending on the amount of spikes fired by the unit in question over the stimulation protocol. For each amount of

spikes that might occur in a stimulation protocol (2 to 4000), we simulated 10000 selectivity indices resulting from random firing (non-selective units). Even though the spikes simulated were random, a lot of SIs fell above the traditional 0.2 threshold. For our data, we thus decided to use a spike-dependent threshold that depends on the number of spikes fired by the unit in question. Such threshold will be the 95th percentile of the histogram distribution of simulated SIs for each particular number of spikes. Fig. S1 shows the resulting threshold curve of the 95th percentile from all these simulations.

Secondly, for comparison with previous literature on orientation selectivity in cats and rodents, we further calculated orientation selectivity indices as the depth of modulation from the preferred orientation to its orthogonal orientation (orthogonal modulation depth index, OMDI; e.g. Niell and Stryker, 2008).

$$OMDI, \theta_{ortho} = \theta_{pref} + {}^{\pi}/_{2}, as\ \frac{R_{pref} - R_{ortho}}{R_{pref} + R_{ortho}} \qquad \text{eq. 2}$$

Thirdly, the shape of orientation and direction tuning curves was also characterized by their half width at half height (HWHH) to be able to compare to previous measures, e.g. in the grey squirrel (Van Hooser et al., 2005). To this end, a single peak Gaussian curve was fitted to the firing rate profiles of neurons with an OSI or DSI > 0.2. For direction HWHH, the curve fitting was done over the twelve stimulation directions. For orientation HWHH, the curve fitting was done over the six orientations of stimulation. This six orientations were obtained by adding together the responses to opposite directions of stimulation (Figure 4).

Orientation preference similarity measures

In order to compare the orientation preference of the neurons across the cortex, we calculated the distance between recording sites in the 250 μm spacing arrays. Single units isolated from the same recording site were considered to be 0 μm apart, neurons in adjacent electrodes were assumed to be either 250 μm or 353 μm apart from each other (for the closest diagonal), and so on.

We implemented two different measures of similarity for orientation selective neurons: (i) the absolute angle difference and (ii) the similarity index based on the correlation of tuning curves.

(i) For every orientation selective unit an angular preference was calculated (Eq. 1). The first measure of similarity between units was therefore the difference in preferred angle. In the orientation space, where preferred angles can only range between 0º and 180º,

this measure goes from 0º (for units with the same preferred orientation angle) to 90º (for units tuned to orthogonal stimuli).

(ii) The firing rate of each orientation selective unit was calculated for each of the 6 stimulation orientations (summing parallel conditions of the 12 directions of movement). Then, for pairwise comparison of units, the Pearson correlation was calculated between the firing rate profiles (analogous to the orientation tuning curve for each unit). This measure ranges from 1 (for units with extremely similar orientation tuning curves) to -1 (for units tuned with orthogonal tuning curves).

When analyzing the statistical significance of these measures, the obtained data points were compared to results from the same analysis for shuffled distances and angles. Comparisons were then made for each data pair (real versus shuffle) using Mann-Whitney tests.

Optical Imaging

Imaging data were pre-processed using custom-made software (OIanalyzer by T. Wunderle) in Matlab. All single condition maps were first-frame corrected at the resolution of frames, blockfiles (all frames for a certain condition in one run of pseudo-randomized conditions) or averaged blockfiles. For the retinotopic imaging, all images were filtered using box-car filters (high-cutoff 50 pixels and low-cutoff 3 pixels) to eliminate illumination and low frequency artifacts. For visualization of compound retinotopy maps, the cortical region responding best to the respective checker bar position was color-coded and the result superimposed on the surface vessel images.

For processing of orientation maps, single condition maps were not filtered. This procedure (zero filter) was adopted to avoid any prior assumption of orientation preference or its regularity. For the construction of ‘angle maps’, activity maps obtained with moving gratings of opposite direction but same orientation were lumped together and frames belonging to the same condition were averaged. Preferred angles of orientation were computed by pixelwise vectorial addition of the activity in the first-frame corrected single-condition maps. For quantification of response selectivity, we further computed the selectivity index (“vector strength” for each pixel) as described for the electrophysiological data above. For visualization, the resulting orientation preference per pixel was color-coded. In order to estimate the coverage of orientation preference in the recorded area we binned all pixels according to their calculated preference orientation in 4 groups of ± 22,5 °.

To test for reliability of the orientation response obtained by optical imaging we started from the notion that responses to the same orientation in different trials should be more

similar to each other than to responses to a different orientation. Thus, we correlated all sum frames (20 repetitions x 8 conditions), within an activated region of interest (stimROI, as deduced from the retinotopic maps), with each other. We did so by repeating the same procedure with only 10% of a randomly drawn subset of the pixels of the stimulated ROI 100 times.

As a further control, we used a shifted ROI region, being illuminated but supposedly not stimulated by the respective monitor position (shiftROI). Additionally, we compared real correlations to those obtained with a sham recording on a rubber brain exposed and illuminated under the same conditions (recording chamber, stimulus monitor, red light source) to exclude systematic correlations induced by correlated camera noise or by stray light from the stimulus monitor during different conditions (lumROI). For each of the correlation procedures, we obtained a profile of mean correlation coefficients per condition as a function of orientation differences.

Experimental Design and Statistical Analyses

The sampling design in the present followed designs classically used for other species, such as cats, and was inspired in cluster sampling of two stages, i.e. the animal and the neuron sampled in the first and second stage, respectively.
The number of simultaneous recording sites per animal (16-48), number of different data sets in different recording depths per animal (2-5), number of trial repetitions (15-20), number of conditions (12 for estimate of orientation preference, 7 for estimate of spatial frequency selectivity), and number of multi- and single units were similar to previous investigations in cats (Wunderle et al., 2013, 2015) and mice (Niell and Stryker, 2008).
Electrophysiology experiments were performed in 11 agoutis and 5 cats (biological replicates). Each of the different gratings was presented 15-20 times per data set in a pseudo-randomized manner for 2000 ms (technical replicate). Per data set we encountered between 25 -50 single units recorded in parallel from the same the animal (biological replicate of electrical activity of different sites recorded simultaneously). We repeated measurements in the same animal after advancing the electrode adding new units from 2 to 8 different data sets (biological replicate of different sites recorded sequentially).
For optical imaging, a common block design repeating the stimulus between 20 and 30 times (technical replicate controlling for systematic influences introduced by camera or monitor noise) while binning two frames per block, was applied for stimulation with 8 different conditions of regions-of-interest (ROI) covering ca. 15.000-18.000 pixels (biological replicate of different cortical sites within the same recording) recording at least two different ROIs (biological replicate of different sites in the same animal recorded in sequence).

The statistical analysis was aimed to provide point estimation and sampling variability of yet undescribed values in agoutis such as receptive field size (mean ± SD, first section of results), orientation selectivity above threshold (Figs. 2, 3), HWHH (Fig. 4) and preference difference across different SFs (Fig. 7).
For statistical tests, we used non-parametric and hence conservative tests with respect to correlations among neurons, responses or pixels from the same animal.
For comparing baseline and evoked activity (firing rate, pre- versus post visual stimulation) we used a Sign test, and only units that passed the test at $p < 0.01$ entered further analyses
In order to test the hypothesis, whether the spatial layout of orientation preference departed from a random layout, the Mann Whitney U test was chosen (Fig. 5, Fig. 6, Figs S4 and S5). The same test was applied to test whether spatial correlations in the intrinsic map were related to the stimulus (Figs 9D and S6). Raw p-values are included in table 1.

References

Conde-Ocazionez, S. A., Jungen, C., Wunderle, T., Eriksson, D., Neuenschwander, N. and Schmidt, K.E. (2018) Callosal Influence on Visual Receptive Fields Has an Ocular, an Orientation-and Direction Bias. Front. Syst. Neurosci. 12, 1–13.

Fiorani, M., Azzi, J. C. B., Soares, J. G. M. and Gattass, R. (2014) Automatic mapping of visual cortex receptive fields: A fast and precise algorithm. J. Neurosci. Methods 221, 112–126.

Niell, C. M. and Stryker, M. P. (2008) Highly selective receptive fields in mouse visual cortex. J. Neurosci. 28, 7520–7536.

Peiker, C., Wunderle, T., Eriksson, D., Schmidt, A. and Schmidt, K. E. (2013) An Updated Midline Rule: Visual Callosal Connections Anticipate Shape and Motion in Ongoing Activity across the Hemispheres. J. Neurosci. 33, 18036–18046.

Quiroga, R. Q., Nadasdy, Z. and Ben-Shaul, Y. (2004) Unsupervised Spike Detection and Sorting with Wavelets and Superparamagnetic Clustering. Neural Comput. 16, 1661–1687.

Skottun, B.C., DeValois, R.L., Grosof, D.H., Movshon, J.A., Albrecht, D.G., Bonds, A.B., 1991. Classifying simple and complex cells on the basis of response modulation. Vis. Res. 31, 1079–1086.

Van Hooser, S. D., Heimel, J. A. and Nelson, S. B. (2005) Functional cell classes and functional architecture in the early visual system of a highly visual rodent. Prog. Brain Res. 149, 127–145.

Wunderle, T., Eriksson, D. and Schmidt, K. E. (2013) Multiplicative mechanism of lateral interactions revealed by controlling interhemispheric input. Cereb. Cortex 23, 900–912.

Wunderle, T., Eriksson, D., Peiker, C. and Schmidt, K.E. (2015) Input and output gain modulation by the lateral interhemispheric network in early visual cortex. J. Neurosci. 35:7682-7694.

Supplemental Information

Table S1: p-values for pairwise angle difference. Related to Figure 5A

Distance (µm)	0	250	354	500	559	707	750	791	901	1061
Cat A18	1.03 e-10	1.49 e-06	0.20	1.47 e-03	8.10 e-07	4.37 e-03	0.15	0.58	6.04 e-05	5.45 e-03
Agouti	3.51 e-13	0.56	0.032	5.46 e-03	0.65	0.30	0.37	0.13	0.72	0.96

Table S2: p-values for pairwise tuning correlation. Related to Figure 5B

Distance (µm)	0	250	354	500	559	707	750	791	901	1061
Cat A18	2.01 e-06	7.01 e-04	0.97	4.47 e-05	8.87 e-11	2.40 e-05	0.24	0.81	0.0012	0.0054
Agouti	1.67 e-06	0.68	0.29	0.59	0.21	0.96	0.18	0.13	0.10	0.29

Table S3: Number of data points per distance (for both, angle difference and tuning correlation). Related to Figure 5

Distance (µm)	0	250	354	500	559	707	750	791	901	1061
Cat A18	46	233	174	129	206	65	51	73	55	15
Agouti	82	599	428	386	577	171	192	287	193	46

Table S4: p-values for vertical and horizontal angle difference and tuning correlation. Related to Figure 6C

Spatial Frequencies (cyc/deg)	0.04	0.08	0.16	0.32	0.64
Angle Difference (SUA)	0.0885	0.0029	1.56 e-07	1.01 e-07	0.0011
Tuning correlation (SUA)	0.3538	08.41 e-04	3..39 e-05	1.16 e-10	4.08 e-03

Table S5: Number of data points for both angle difference and tuning correlation. Related to Figure 6C

Spatial Frequencies (cyc/deg)	0.04	0.08	0.16	0.32	0.64

N vertical	112	508	480	248	280
N horizontal	2286	2389	1864	1935	1494

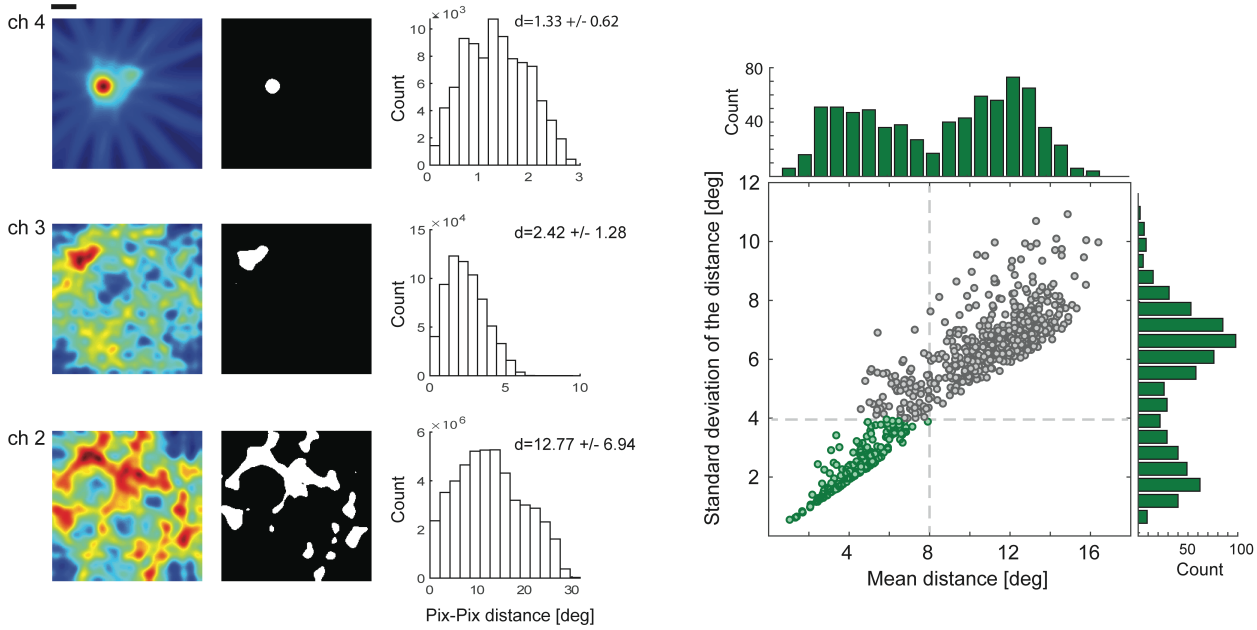

Figure S1: Selection of well-defined receptive fields. Related to Figure 1.

A: Examples of three receptive field map candidates (left column). Binary maps considering only pixels above 0.7 (white areas, center column) and distribution of pair-wise distances *d* between these pixels (right column) characterized by their mean +/- standard deviation. Scale bar: 5 degrees.

B: Distributions of mean and standard deviation values from all potential receptive field maps across all animals. Gray traced lines correspond to the defined thresholds. Receptive fields maps associated with green dots were considered for further analysis. Receptive fields maps associated with gray dots were not considered.

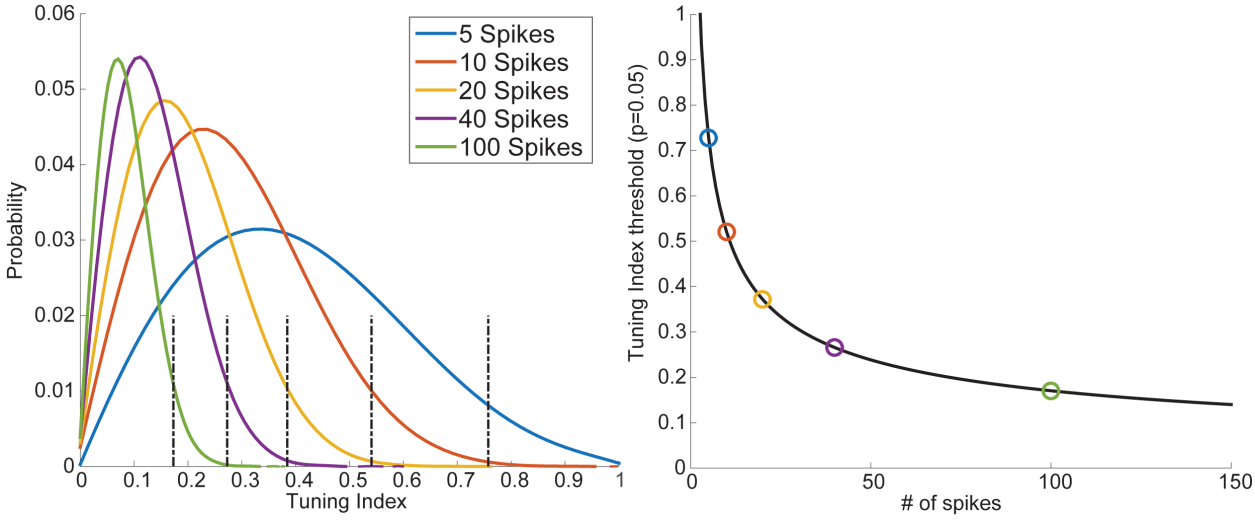

Figure S2: Spike-dependent selectivity index threshold simulations. Related to Figure 2.

A: Histogram of Selectivity Indices for 10000 simulations of randomly distributed spikes. Black vertical dotted lines depict the 95th percentile threshold for each distribution (p=0.05). B: 95th percentile TI threshold versus number of spikes. Black circles depict the thresholds for the simulations in A.

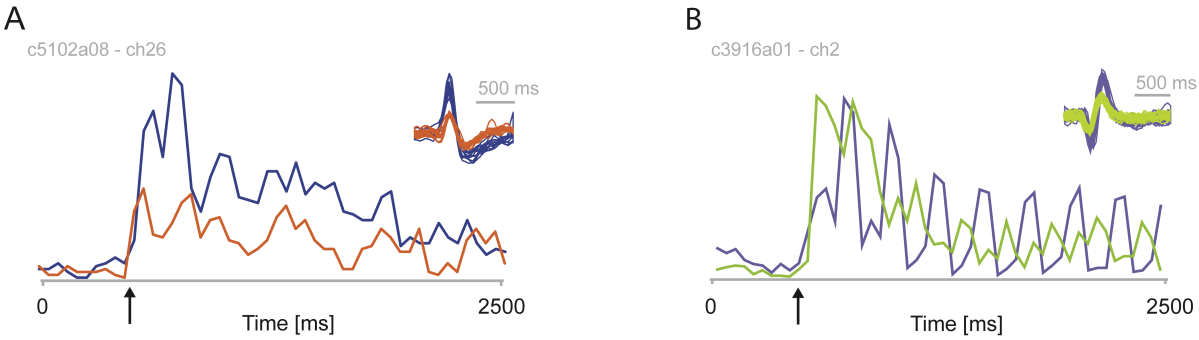

Figure S3: Peri-stimulus time histogram (PSTH) examples. Related to Figure 2.

A, agouti PSTHs, and B, cat PSTHs, from the units depicted in Figure 2A and 2B, respectively. Similarly tuned but separable waveforms (inset) could be isolated from multi-units in both species.

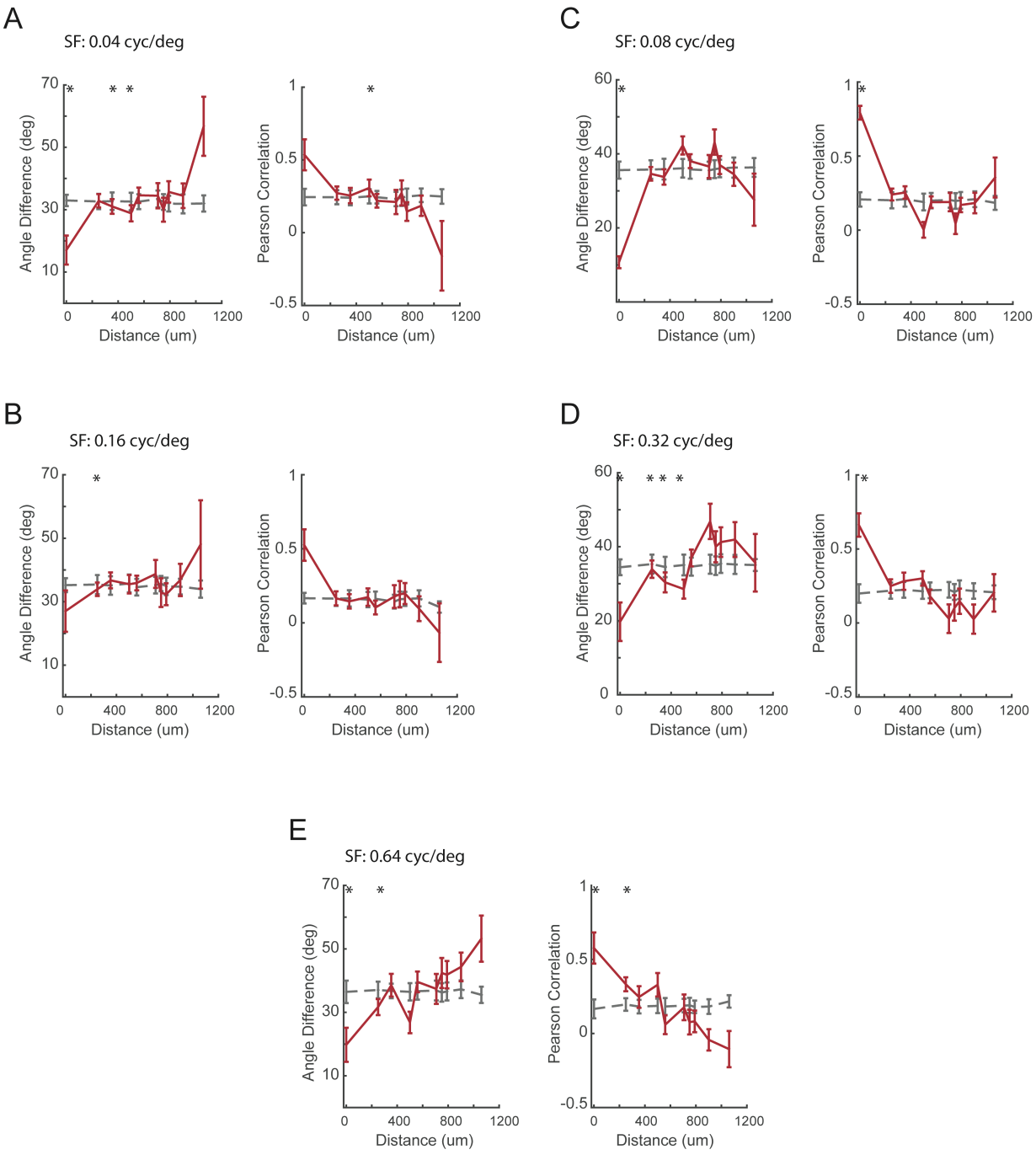

Figure S4: Spatial layout of orientation selective neurons in the horizontal axis separated by spatial frequency (SF). Related to Figure 5.

Tuning difference between cell pairs as a function of distance (red). Since in agouti, orientation preference changes with spatial frequency, differences were calculated from the orientation preference angle obtained at different SFs separately. Asterisks depict significant differences between the correlations obtained for recorded (red) and shuffled data (dotted grey).

Significance criterion: Mann-Whitney p<0.001 Note that the tendency of similar preferences to cluster locally is preserved. Error bars are SEM.

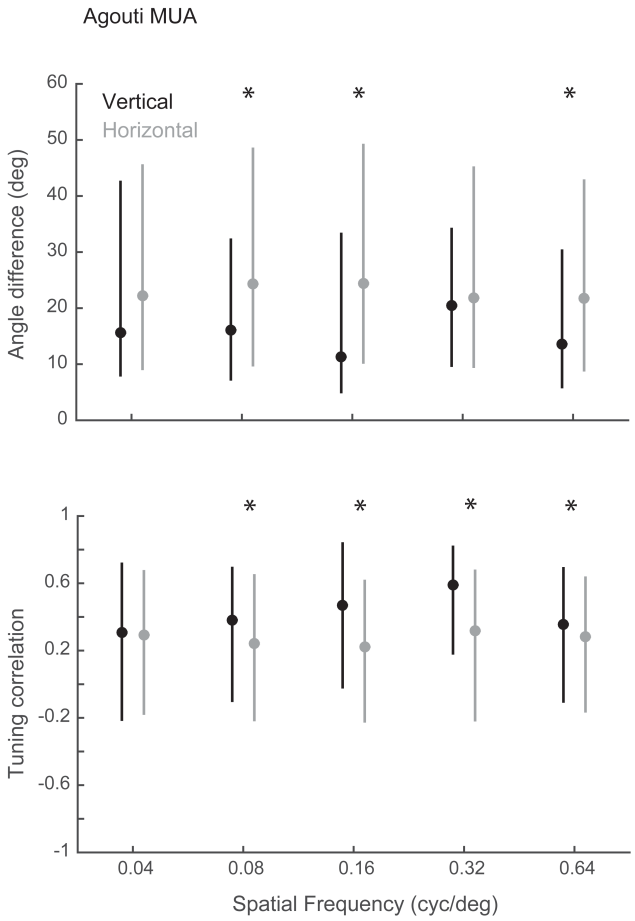

Figure S5: Pairwise comparisons of orientation preference of multi-unit activity (MUA). Related to Figure 6C.

Median and interquartile ranges are depicted by circles and lines, respectively. Empty and filled circles depict pairwise comparisons between MUA activity of sites from Neuronexus probes or electrode arrays, respectively. Probe electrodes sample from a vertical cylinder (orthogonal to cortical surface). Arrays sample from horizontal planes (parallel to cortical surface). Angle difference (top) and tuning similarity (bottom). Both measures indicate a greater similarity between multi-units arranged vertically. * depicts p<0.0001 (Mann-Whitney U test). Probe electrode data from 3 agoutis. Array electrode data from 5 agoutis.

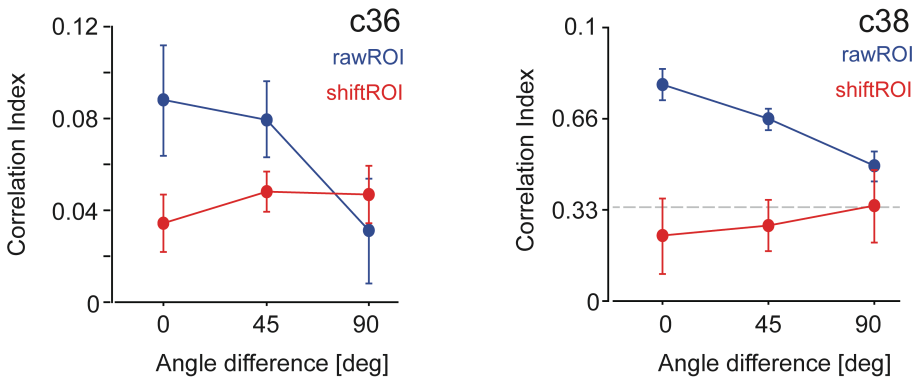

Figure S6. Mean spatial correlation coefficients between all summed frames. Related to Figure 9.

Spatial correlation within the stimulated ROI (blue), and shifted ROI in a not stimulated area (red) for agouti C36. Distributions of correlation coefficients in different angle difference compartments were statistically compared (Mann-Whitney-U test, difference between group 0 vs 90: n = 1020, stimROI, p = 0.0046; shiftROI, p = 0.48) and C38 (Mann-Whitney-U test, difference between group 0 vs 90: n = 3120, stimROI, p = 0.0001; shiftROI, p =0.57).